

MEASURING BARYON ACOUSTIC OSCILLATIONS ALONG THE LINE OF SIGHT WITH PHOTOMETRIC REDSHIFTS: THE PAU SURVEY

N. BENÍTEZ¹, E. GAZTAÑAGA², R. MIQUEL^{3,4}, F. CASTANDER², M. MOLES⁵, M. CROCCE², A. FERNÁNDEZ-SOTO^{6,7}, P. FOSALBA², F. BALLESTEROS⁸, J. CAMPA⁹, L. CARDIEL-SAS⁴, J. CASTILLA⁹, D. CRISTÓBAL-HORNILLOS⁵, M. DELFINO¹⁰, E. FERNÁNDEZ¹³, C. FERNÁNDEZ-SOPUERTA², J. GARCÍA-BELLIDO¹¹, J. A. LOBO², V. J. MARTÍNEZ⁸, A. ORTIZ⁸, A. PACHECO^{4,10}, S. PAREDES^{8,14}, M. J. PONS-BORDERÍA^{8,15}, E. SÁNCHEZ⁹, S. F. SÁNCHEZ¹², J. VARELA⁵, AND J. F. DE VICENTE⁹

¹ Instituto de Matemáticas y Física Fundamental (CSIC), Madrid, Spain

² Institut de Ciències de l’Espai (IEEC-CSIC), Barcelona, Spain

³ Institució Catalana de Recerca i Estudis Avançats, Barcelona, Spain

⁴ Institut de Física d’Altes Energies, Barcelona, Spain

⁵ Instituto de Astrofísica de Andalucía (CSIC), Granada, Spain

⁶ Departament d’Astronomia i Astrofísica, Universitat de València, Spain

⁷ Instituto de Física de Cantabria (CSIC), Santander, Spain

⁸ Observatori Astronòmic de la Universitat de València, Spain

⁹ Centro de Investigaciones Energéticas, Medioambientales y Tecnológicas, Madrid, Spain

¹⁰ Port d’Informació Científica, Barcelona, Spain

¹¹ Instituto de Física Teórica (UAM-CSIC), Madrid, Spain

¹² Centro Astronómico Hispano Alemán (CSIC/MPG), Calar Alto, Spain

Received 2008 July 18; accepted 2008 September 21; published 2009 January 9

ABSTRACT

Baryon Acoustic Oscillations (BAOs) provide a “standard ruler” of known physical length, making it one of the most promising probes of the nature of dark energy (DE). The detection of BAOs as an excess of power in the galaxy distribution at a certain scale requires measuring galaxy positions and redshifts. “Transversal” (or “angular”) BAOs measure the angular size of this scale projected in the sky and provide information about the angular distance. “Line-of-sight” (or “radial”) BAOs require very precise redshifts, but provide a direct measurement of the Hubble parameter at different redshifts, a more sensitive probe of DE. The main goal of this paper is to show that it is possible to obtain photometric redshifts with enough precision (σ_z) to measure BAOs along the line of sight. There is a fundamental limitation as to how much one can improve the BAO measurement by reducing σ_z . We show that $\sigma_z \sim 0.003(1+z)$ is sufficient: a much better precision will produce an oversampling of the BAO peak without a significant improvement on its detection, while a much worse precision will result in the effective loss of the radial information. This precision in redshift can be achieved for bright, red galaxies, featuring a prominent 4000 Å break, by using a filter system comprising about 40 filters, each with a width close to 100 Å, covering the wavelength range from ~ 4000 to ~ 8000 Å, supplemented by two broad-band filters similar to the Sloan Digital Sky Survey u and z bands. We describe the practical implementation of this idea, a new galaxy survey project, PAU¹⁶, to be carried out with a telescope/camera combination with an *etendue* about 20 m² deg², equivalent to a 2 m telescope equipped with a 6 deg² field of view camera, and covering 8000 deg² in the sky in four years. We expect to measure positions and redshifts for over 14 million red, early-type galaxies with $L > L_*$ and $i_{AB} \lesssim 22.5$ in the redshift interval $0.1 < z < 0.9$, with a precision $\sigma_z < 0.003(1+z)$. This population has a number density $n \gtrsim 10^{-3}$ Mpc⁻³ h^3 galaxies within the 9 Gpc³ h^{-3} volume to be sampled by our survey, ensuring that the error in the determination of the BAO scale is not limited by shot noise. By itself, such a survey will deliver precisions of order 5% in the dark-energy equation of state parameter w , if assumed constant, and can determine its time derivative when combined with future cosmic microwave background measurements. In addition, PAU will yield high-quality redshift and low-resolution spectroscopy for hundreds of millions of other galaxies, including a very significant high-redshift population. The data set produced by this survey will have a unique legacy value, allowing a wide range of astrophysical studies.

Key words: cosmological parameters – large-scale structure of universe

Online-only material: color figures

1. INTRODUCTION

Physical cosmology has recently entered the precision era. This transition has been propelled by the gathering, over the past decade, of unprecedented high-precision data sets for several cosmological observables. The combined analysis of the cosmic

microwave background (CMB) anisotropies (e.g., Spergel et al. 2007; Komatsu et al. 2008; Jones et al. 2006; Readhead et al. 2004; Reichardt et al. 2008; Dickinson et al. 2004) with distance-scale measurements at increasingly higher redshifts (e.g., Wood-Vasey et al. 2007; Astier et al. 2006; Riess et al. 2007) and probes of large-scale structure (Cole et al. 2005; Tegmark et al. 2004, 2006; Percival et al. 2007; Hütsi 2006b) yields a remarkably consistent picture: a spatially flat universe that has started a phase of acceleration of the expansion at the present epoch. From the observations gathered so far this acceleration is consistent with the effect of a cosmological constant, but it may

¹³ PAU Coordinator. Enrique.Fernandez@ifae.es.

¹⁴ Permanent address: Universidad Politécnica de Cartagena, Spain.

¹⁵ Permanent address: Universidad Complutense de Madrid, Spain.

¹⁶ Physics of the Accelerating Universe (PAU): <http://www.ice.cat/pau>.

also be caused by the presence of a dynamical energy component with negative pressure, now termed dark energy (DE), or might also point to a fundamental modification of our description of gravity. The answer to what is the exact cause is likely to have profound implications for cosmology and for particle physics.

Two recent collective reports, one by the US Dark Energy Task Force (DETF; Albrecht et al. 2006), convened by NASA, NSF, and the Department of Energy, and another by the European ESA-ESO Working Group on Fundamental Cosmology (Peacock et al. 2006), have identified the most promising observational strategies to characterize DE properties in the near future. These reports concluded that the method based on measurements of Baryon Acoustic Oscillations (BAOs) from galaxy redshift surveys is less likely to be limited by systematic uncertainties than other methods that are proposed. It appears that, while recognizing the need for a combined strategy involving two or more independent techniques, BAO measurements can substantially contribute to increase the accuracy on the DE equation of state.

BAOs are produced by acoustic waves in the photon–baryon plasma generated by primordial perturbations (Eisenstein & Hu 1998). At recombination ($z \sim 1100$), the photons decouple from the baryons and start to free stream, whereas the pressure waves stall. As a result, baryons accumulate at a fixed distance from the original overdensity. This distance is equal to the sound horizon length at the decoupling time, r_{BAO} . The result is a peak in the mass correlation function at the corresponding scale. First detections of this excess were recently reported, at a significance of about three standard deviations, both in spectroscopic (Eisenstein et al. 2005; Percival et al. 2007b; Hütsi 2006a) and photometric (Padmanabhan et al. 2007; Blake et al. 2007) galaxy redshift surveys.

The comoving BAO scale is accurately determined by CMB observations ($r_{\text{BAO}} = 146.8 \pm 1.8$ Mpc for a flat Λ CDM universe; Hinshaw et al. 2008), and constitutes a “standard ruler” of known physical length. The existence of this natural standard ruler, measurable at different redshifts, makes it possible to probe the expansion history of the universe, and thereby DE properties and the universe geometry (see e.g., Seo & Eisenstein 2003; Blake & Glazebrook 2003 and references therein). This motivates the present efforts to measure BAO (e.g., ADEPT 2008; DES 2008; HETDEX 2008; Pan-STARRS 2008; SPACE 2008; Basett et al. 2005; WiggleZ 2008).

Broad-band photometric galaxy surveys can measure the angular scale of r_{BAO} in several redshift shells, thereby determining $d_A(z)/r_{\text{BAO}}$, where $d_A(z)$ is the angular distance to the shell at redshift z . If galaxy redshifts can be determined precisely enough, the BAO scale can also be measured along the line of sight, providing a direct measurement of the instantaneous expansion rate, the Hubble parameter (or actually of $H(z)r_{\text{BAO}}$), at different redshifts. This quantity is more sensitive to the matter-energy contents of the universe compared with the integrated quantity $d_A(z)$. The direct determination of $H(z)$ distinguishes the BAO method from other methods. In addition, since systematic errors affect the radial and tangential measurements in different ways, the consistency between the measured values of $H(z)$ and $d_A(z)$ offers a test of the results.

As a rule of thumb, in order to get the same sensitivity to the dark-energy parameters, a galaxy redshift survey capable of exploiting the information along the line of sight needs to cover only $\sim 10\%$ of the volume covered by a comparable survey that detects the scale in the transverse direction only (Blake & Bridle 2005). When covering a similar volume, precise enough redshift

measurements can provide substantially tighter constraints on the DE parameters.

Large volumes have to be surveyed in order to reach the statistical accuracy needed to obtain relevant constraints on dark-energy parameters. Enough galaxies must be observed to reduce the shot noise well below the irreducible component due to sampling variance (see Section 2.4). The usefulness of the correlation along the line of sight favors spectroscopic redshift surveys that obtain very accurate redshifts, but the need for a large volume favors photometric redshifts that can reach down to fainter galaxies.

The intrinsic comoving width of the peak in the mass correlation function is about $15 \text{ Mpc } h^{-1}$, due mostly to Silk damping (Silk 1968). This sets a requirement for the redshift error of order $\sigma(z) = 0.003(1+z)$, corresponding to $15 \text{ Mpc } h^{-1}$ along the line of sight at $z = 0.5$. A much better precision will result in oversampling of the peak without a substantial improvement on its detection, while worse precision will, of course, result in the effective loss of the information in the radial modes (Seo & Eisenstein 2003). Note also that in the presence of substantial redshift errors, the error distribution needs to be known and accurately corrected for when inferring the BAO scale.

It has usually been assumed in the literature that photometric redshifts are not precise enough to measure “line-of-sight” BAOs (Seo & Eisenstein 2003; Blake & Bridle 2005). While this is true for broad-band photometric surveys, here we examine how one can reach the required redshift precision with narrow-band photometry. We find (see Section 3) that redshifts of luminous red galaxies (LRGs) can be measured with a precision $\sigma(z) \sim 0.003(1+z)$ using a photometric system of 40 filters of $\sim 100 \text{ \AA}$, continuously covering the spectral range from ~ 4000 to $\sim 8000 \text{ \AA}$, plus two additional broad-band filters similar to the u and z bands.

We describe the practical implementation of this idea, a photometric galaxy redshift survey called PAU (Physics of the Accelerating Universe). PAU will measure positions and redshifts for over 14 million LRGs over 8000 deg^2 in the sky, in the range $0.1 < z < 0.9$ (comprising a volume of $9 \text{ Gpc}^3 h^{-3}$), and with an expected photometric redshift precision $\sigma(z) \lesssim 0.003(1+z)$. This redshift precision makes it possible to measure radial BAO with minimal loss of information. The PAU Survey can be carried out in a four year observing program at a dedicated telescope with an effective *etendue* $\sim 20 \text{ m}^2 \text{ deg}^2$.

The outline of the paper is as follows. Section 2 discusses the scientific requirements for such a survey. An optimization of the survey parameters follows in Section 3, while Section 4 presents a possible baseline design for the instrument. The science capabilities of the survey are given in Section 5. Finally, Section 6 contains the summary and conclusions.

2. SCIENTIFIC REQUIREMENTS

Given current priors on other cosmological parameters a measurement of the expansion rate history $H(z)$ with percent precision will translate into a measurement of the DE equation of state w of few times this precision. We will focus here on how well we can do this by measuring the BAO feature at comoving size $r_{\text{BAO}} \simeq 100 \text{ Mpc } h^{-1}$ and use it as a standard ruler in both the radial and tangential directions.

We first explore how an error in the BAO scale r_{BAO} translates into an error in the DE equation of state w . The relation is

different if we measure the scale in the radial or tangential (i.e., angular) direction. We then move to show how the BAO scale can be measured statistically using galaxy surveys. We start with a visual illustration of the problem and a brief presentation of two N -body simulations that we used in order to study the main goal of this paper. We then show how this scale can be measured using the statistics of galaxy density fluctuations and relate the error in r_{BAO} to the volume of the survey, given perfect distance indicators. We finish by considering what redshift precision is required to maintain a given precision in the r_{BAO} measurement and how this is limited by different systematic effects. Note that we focus here in showing the implication of the photo- z accuracy in the measurements of the monopole, which combines the radial and perpendicular information. These two components can be separated by considering the anisotropic correlation function (see Okumura et al. 2008; Padmanabhan & White 2008; Cabre & Gaztanaga 2008; and Figures 17 and 18 in Gaztanaga et al. 2008, which show how the anisotropic correlation function changes for PAU-like photo- z precisions).

We note that these are just rough estimates to show the viability of this approach. In a real survey, there might be other sources of systematic errors that have not been taken into account in detail here. However, experience indicate that the actual data themselves can be used to study and minimize those sources of errors.

In what follows we assume a flat FRW cosmology, with cosmological parameters compatible with *Wilkinson Microwave Anisotropy Probe* (WMAP) data (Hinshaw et al. 2008).

2.1. BAO Scale and DE Equation of State

In a galaxy survey we measure distances in terms of angles and redshifts. These observed quantities can be related to known distances, such as r_{BAO} , using the FRW metric. The differential radial (comoving) distance is inversely proportional to the expansion rate $H(z) \equiv \dot{a}/a$:

$$dr(z) = \frac{c}{H(z)} dz, \quad (1)$$

while the angular diameter distance is proportional to the integral of $dr(z)$:

$$d_A(z) = \frac{c}{1+z} \int_0^z \frac{dz'}{H(z')} \quad (2)$$

for a flat universe. In particular, measurements of the characteristic size of the BAO feature in the radial (δz_{BAO}) and tangential ($\delta\theta_{\text{BAO}}$) direction relate to the known comoving BAO scale r_{BAO} as

$$\delta z_{\text{BAO}} = r_{\text{BAO}} \frac{H(z)}{c}, \quad (3)$$

$$\delta\theta_{\text{BAO}} = \frac{r_{\text{BAO}}}{d_A(z)(1+z)}. \quad (4)$$

We therefore have, neglecting for a moment the uncertainty on the determination of r_{BAO} by CMB observations, that a relative error in the measured size of the BAO feature corresponds to a relative error in either $d_A(z)$ or $H(z)$:

$$\begin{aligned} \Delta_{\text{BAO}}^T &\equiv \frac{\sigma(\delta\theta_{\text{BAO}})}{\delta\theta_{\text{BAO}}} = \frac{\Delta d_A}{d_A}, \\ \Delta_{\text{BAO}}^L &\equiv \frac{\sigma(\delta z_{\text{BAO}})}{\delta z_{\text{BAO}}} = \frac{\Delta H}{H}. \end{aligned} \quad (5)$$

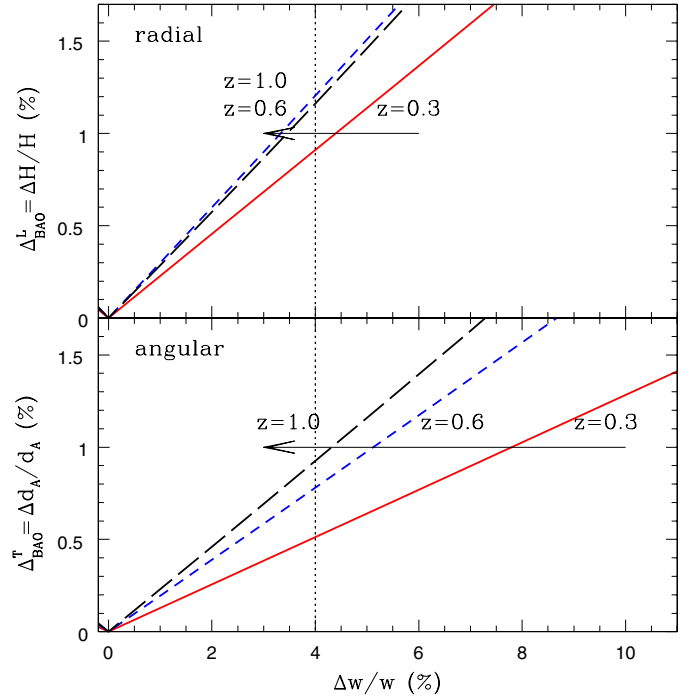


Figure 1. Relation between the change in the DE equation of state parameter w , shown in the x -axis, and its effect in the apparent measured BAO scale, Δ_{BAO} , shown in the y -axis. Changes are shown in percent, relative to the $w = -1$ case. Top panel corresponds to the radial distance: $\Delta_{\text{BAO}}^L = \Delta H(z)/H(z)$. The bottom panel shows the angular diameter distance: $\Delta_{\text{BAO}}^T = \Delta d_A(z)/d_A(z)$. The different lines correspond to $z = 0.3$ (continuous), $z = 0.6$ (short dashed), and $z = 1$ (long dashed). In all cases $\Omega_m = 0.25$ and flat universe are assumed. All other cosmological parameters are kept fixed.

(A color version of this figure is available in the online journal.)

For this argument, we will write the expansion rate as

$$H^2(z)/H_0^2 = \Omega_m (1+z)^3 + (1 - \Omega_m) (1+z)^{3(1+w)} \quad (6)$$

which corresponds to a flat universe ($\Omega_m + \Omega_{\text{DE}} = 1$) with a constant equation of state $w \equiv p/\rho$, with p the pressure and ρ the density of the DE. Figure 1 shows the relative change in Equation (5) (in percent) as a function of the relative changes in w with respect to $w = -1$ for different redshifts. We show the cases for $z = 0.3$ – 1.0 , which will be relevant for our study. As can be seen in the figure, a 1% error in Δ_{BAO} (our goal) at $z \simeq 1.0$ results in a $\simeq 4\%$ uncertainty in w , but the precision varies with redshift. A constant 1% error in the angular distance quickly degrades the w precision with decreasing redshift, from 4.5% at $z = 1.0$ to 8.0% at $z = 0.3$, while the radial distance achieves a more uniform precision in w , 3.5%–4.5% in the whole redshift range.

This illustrates the advantage of having a good radial measurement. Angular distances provide a good geometrical test, while radial distances tell us directly the instantaneous expansion rate. In addition, comparing relative sizes of the BAO feature when measured parallel and perpendicular to the line of sight will provide us with a consistency test.

2.2. BAO Scale in N -Body Simulations

To support some of the main claims of this paper we have used large N -body dark matter (DM) simulations, using the MICE collaboration¹⁷ setup. In particular, we have computed

¹⁷ <http://www.ice.cat/mice>

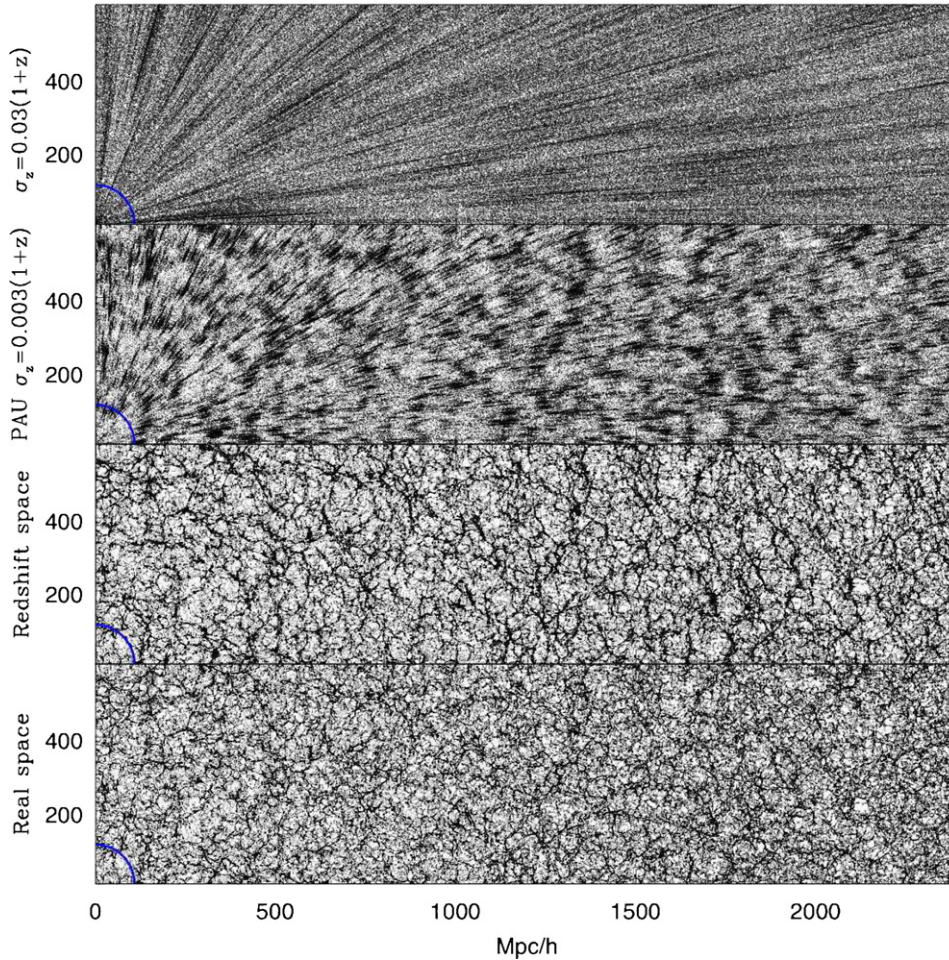


Figure 2. Systematic effects in the light cone: panels show a $1 \text{ Mpc } h^{-1}$ thick section of the light cone distribution in MICE3072 in comoving coordinates. The two bottom panels corresponds to the actual DM distribution in the simulation in real (bottom) and redshift space (upper panels). The top two panels also include a (Gaussian distributed) photo- z error distortion of $\sigma_z = 0.003(1+z)$, as expected from PAU galaxies, and an order-of-magnitude worse case, $\sigma_z = 0.03(1+z)$. The BAO scale is shown by a section of circle with radius $100 \text{ Mpc } h^{-1}$ around the observer.

(A color version of this figure is available in the online journal.)

nonlinear DM clustering statistics in terms of the two-point correlation function, $\xi(r)$, and its Fourier transform, the power spectrum, $P(k)$, and we have assessed the impact of real world systematic effects on the BAO measurements based on these standard estimators.

MICE simulations have been run using the Gadget-2 code (Springel 2005) on the MareNostrum supercomputer at BSC,¹⁸ with a modification to produce outputs in the light cone (Fosalba et al. 2007). We focus here on two simulations, shown in Table 1, corresponding to a flat concordance Λ CDM model with $\Omega_m = 0.25$, $\Omega_\Lambda = 0.75$, $\Omega_b = 0.044$, $n_s = 0.95$, $\sigma_8 = 0.8$, and $h = 0.7$. Halos were obtained from the $z = 0.5$ comoving output using the friends-of-friends (FoF) algorithm with linking length 0.164. The larger simulation has a dynamic range close to 5 orders of magnitude.

Figure 2 shows a thin slice of the light cone built from the MICE3072 simulation. We build the light cone placing the observer at the origin, so that cosmic time (redshift) corresponds to the radial direction, which expands from $z = 0$ to $z = 1$ (corresponding to a comoving radius of $2400 \text{ Mpc } h^{-1}$ for our cosmology). The bottom panel corresponds to the true DM distribution in real space. The second panel from the

Table 1
N-Body Simulations Used in this Paper

Name Acronym	L_{box} ($\text{Mpc } h^{-1}$)	N_{par} Number	Halo Mass ($10^{11} M_{\text{sun}} h^{-1}$)	N_{halos} Total Number
MICE3072	3072	1024^3	>375	1.1×10^6
MICE1536	1536	1024^3	>47	2.1×10^6

Note. Minimum halo mass and number of halos correspond to $z = 0.5$.

bottom panel shows the redshift space distribution where the radial positions are distorted due to peculiar (gravitationally induced) motions away from the Hubble flow. In order to model this distortion, we add the radial component of the peculiar velocity v_r of each particle to its (real space) position: $s = r + f v_r (1+z)/H(z)$, where $f \sim 1$ for the assumed Λ CDM cosmology at $z \sim 0.5$. We note that, in this image, distortions can only be seen whenever they are much larger than the pixel size $\Delta r_{\text{pix}} \simeq 3 \text{ Mpc } h^{-1}$ or, in velocity units, $\Delta v_{\text{pix}} \simeq 300 \text{ km } s^{-1}$. This implies that the so-called fingers-of-God effect (see explanation below) cannot be detected because it arises from random peculiar velocities of order Δv_{pix} . Instead, the Kaiser effect (Kaiser 1987) due to a large-scale coherent infall is visible as an enhancement of the filamentary structures perpendicular to the line of sight.

¹⁸ Barcelona Supercomputer Center, <http://www.bsc.es>.

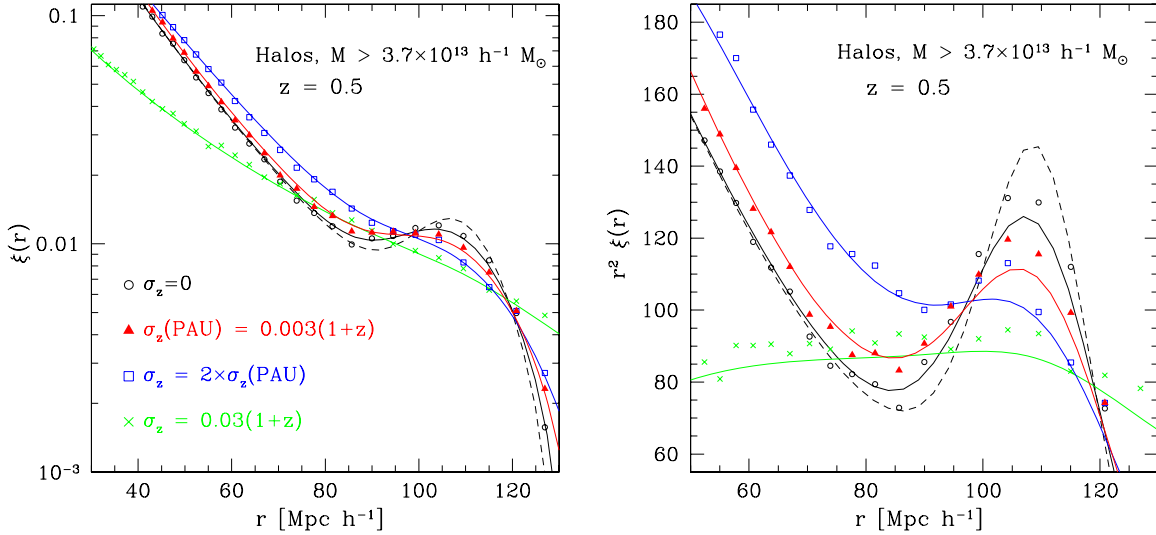


Figure 3. Smearing of the BAO signature due to photometric redshift errors. The circles denote the two-point correlation function from over a million halos with mass $M > 3.7 \times 10^{13} h^{-1} M_{\odot}$ (assumed to host LRGs) measured in a MICE simulation of $27 h^{-3} \text{Gpc}^3$ volume. The dashed line is the linear correlation function scaled with the linear halo bias ($b = 3$), while the black solid line corresponds to the nonlinear prediction given by RPT (Crocce & Scoccimarro 2008). Their difference shows the degradation coming solely from nonlinear clustering. In addition, the triangle (red), square (blue), and cross (green) symbols show the measured correlation function after a Gaussian error degradation in the line-of-sight position of the halos is introduced ($\sigma_z/(1+z) = 0.003, 0.007, \text{ and } 0.03$, respectively). The corresponding solid lines are the analytical predictions derived from Equation (8). The right panel shows a zoom over the peak region scaled as $r^2\xi(r)$. Clearly, the S/N in the BAO feature reduces with photo- z error and starts to totally disappear above the PAU threshold of 0.003, which roughly corresponds to the intrinsic width of the BAO feature due to Silk damping.

(A color version of this figure is available in the online journal.)

The two top panels also include a radial distortion due to photo- z errors which we assumed to be Gaussian distributed. Thus, they can be modeled by randomly displacing the particles along the line of sight according to the probability distribution,

$$f(\delta r_z) \sim \exp[-(1/2)(\delta r_z/\Delta_z)^2], \quad (7)$$

with the smoothing scale Δ_z and the photo- z error σ_z related through the Hubble parameter $H(z)$ as $\Delta_z = \sigma_z(1+z)c/H(z)$. Third panel up assumes $\sigma_z = 0.003(1+z)$, which is roughly the photo- z error expected for PAU galaxies, while the top panel corresponds to an order-of-magnitude worse case, $\sigma_z = 0.03(1+z)$.

Overall this figure illustrates how the image is degraded both by peculiar velocities and redshift errors. Comparing the middle panels, it is evident that redshift errors produce, on average, much stronger distortions than peculiar velocities.

2.3. Redshift Errors

We now turn to a more quantitative estimate of the minimum radial resolution required to detect the BAO scale in 3D.

The BAO signature appears in the two-point correlation of particles as a single bump at a scale $r_{\text{BAO}} \simeq 100 h^{-1} \text{Mpc}$ with an intrinsic width $\Delta r_{\text{BAO}} \simeq 10 h^{-1} \text{Mpc}$ and relative amplitude of about a factor of 2 with respect to a non-BAO model with the same broad-band shape. Therefore, a simple approach would be to look at the degradation of this peak as we increase the redshift error.

To be more realistic, we have studied the clustering of halos (selected with an FoF algorithm with linking length of 0.164) since they are more closely related to the observed galaxies and clusters of galaxies than DM particles. In particular, LRGs are thought to populate large DM halos and closely trace the halo distribution.

At large scales the halo and matter density fluctuations are related by a linear bias factor ($\delta_{\text{halo}} = b \delta_{\text{matter}}$), which translates into a b^2 scaling for the two-point function. Halos with large mass cut in Table 1 have $b \simeq 3$, which was chosen to magnify possible nonlinear effects. To estimate errors, we use instead a lower mass cut which corresponds to $b \simeq 2$ and better matches the clustering of LRGs that have already been used to measure BAOs (e.g., Eisenstein et al. 2005; Tegmark et al. 2006).

Figure 3 shows the two-point correlation function (black empty circles) traced by all halos in MICE3072 at $z = 0.5$ (see Table 1). The dashed line corresponds to the linear correlation and the black solid line to the nonlinear model of Renormalized Perturbation Theory (RPT; Crocce & Scoccimarro 2008), both biased with $b = 3$. As illustrated by Figure 3 (solid black line), the simple scale-independent linear bias scheme works reasonably well, but this assumption certainly needs to be tested more accurately.

We then estimated the impact of photo- z errors using Gaussian distortions in the radial direction as described in the previous section. The corresponding correlation function of this smeared distribution of halos is shown in Figure 3 for different values of the photo- z error, $\sigma_z/(1+z) = 0.003$ (as expected for PAU), 0.006, and 0.03, with red, blue, and green symbols, respectively.

In turn, this smearing can be modeled in Fourier space by damping the power spectrum along the line of sight as

$$P_z(k, \mu) = b^2 P_{nl}(k) \exp[-k^2 \Delta_z^2 \mu^2], \quad (8)$$

where P_{nl} is the nonlinear power spectrum from RPT, the linear bias is $b = 3$, and μ is the cosine of the angle with the line of sight. The red, blue, and green solid lines in Figure 3 correspond to the angle-averaged Fourier transform of Equation (8) for $\sigma_z = 0.003, 0.006, \text{ and } 0.03$, respectively.

In summary, Figure 3 illustrates that one can basically recover the right BAO shape once the error is better than about

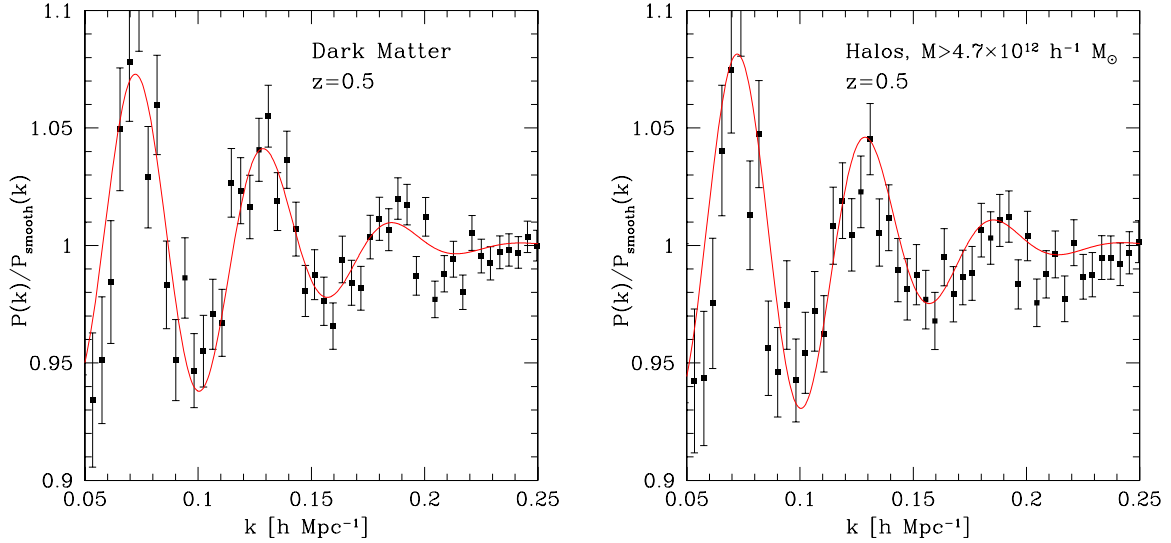


Figure 4. Ratio of the power spectrum measured at $z = 0.5$ in MICE1536 to a smoothed version of the same spectrum for DM (left panel) and halos of mass $M \geq 4.7 \times 10^{12} h^{-1} M_{\odot}$ (right panel). These large halos are expected to host LRGs. The reference spectrum was obtained by rebinning the original one in bins of $\Delta k = 0.055 h \text{ Mpc}^{-1}$ in order to wash out the BAO signature but keeping the broad-band shape of the nonlinear spectrum. Error bars were obtained using the approximation in Equation (9). The red solid line corresponds to the parametric fit given by Equation (10) with $A/r_{\text{BAO}} = 0.016$ for DM and $A/r_{\text{BAO}} = 0.017$ for halos ($r_{\text{BAO}} = 108.6 \text{ Mpc } h^{-1}$ for our reference cosmology). This figure illustrates that for both DM and halos, one can approximately model BAO in the $P(k)$ with Equation (10). This conclusion also applies in redshift space and for different galaxy populations (Angulo et al. 2008).

(A color version of this figure is available in the online journal.)

$0.003(1+z)$. Larger errors erase the BAO bump and will result in the loss of cosmological information. The change can be roughly quantified by the ratio between the amplitude of the BAO peak (at $r \simeq 108 \text{ Mpc } h^{-1}$) and the amplitude in the valley (at $r \simeq 85 \text{ Mpc } h^{-1}$). For $r^2 \xi(r)$ in the right panel of Figure 3, this ratio is about 1.8 in real space with no photometric errors and decreases smoothly to 1.5 as we increase the error toward $0.003(1+z)$. For larger errors, this ratio decreases more rapidly and gets all the way to unity for $0.006(1+z)$, as shown in the figure. This makes sense because $0.003(1+z)$ corresponds to a comoving scale of about $15 h^{-1} \text{ Mpc}$ at $z = 0.5$, which matches the intrinsic width (Silk damping) of the BAO peak. Although this is just a rough estimate, it is all we need as a starting point for our considerations below, and it agrees with other considerations based on counting the number of modes in two-dimensional and three-dimensional surveys and the work of Blake & Glazebrook (2003) and Seo & Eisenstein (2003).

The clustering analysis presented above is in real rather than redshift space. Redshift space distortions can be modeled as a combination of two separate effects: coherent and random peculiar velocities. The first term is the so-called Kaiser effect (Kaiser 1987), which increases the amplitude of clustering at large scales by a factor of $\sim (1 + \beta \mu^2)^2$ (where $\beta = \Omega_m^{0.6}/b$, b is the bias and μ is the cosine of the angle with the line of sight). Our analysis allows for such an effect by incorporating a larger effective bias in the correlation function monopole (e.g., $b = 3$ as in Figure 3). The effect of random velocities can be modeled as a Gaussian damping, very similar to photo- z errors in Equation (8) but where σ_z^2 is replaced by $\sigma_p^2/2$, where σ_p is the one-dimensional galaxy pairwise velocity dispersion (the factor of 1/2 is because a velocity difference has twice the variance of a single velocity). The net effect is that the density field is convolved with a one-dimensional random field with a net dispersion $\sigma^2 = \sigma_p^2/2 + \sigma_z^2$. The typical value of σ_p in our DM simulation is smaller than the photo- z errors considered here. This is also the case in regions of high density, populated by LRG galaxies, and where σ_p could be larger, e.g.,

$\sigma_p \sim 400 \text{ km s}^{-1}/c \sim 0.0013$ for $r > 5 \text{ Mpc } h^{-1}$ (Ross et al. 2007). This is clearly seen by comparing the two middle panels of Figure 2 where it is evident that even in regions of high density the photo- z distortions are larger than the redshift space distortions. Thus, effectively $\sigma_z > \sigma_p$ and we can consider this effect subdominant in our considerations.

We note here that there is a fundamental limitation as to how much one can improve the BAO measurement by reducing the photo- z error. The photo- z error $\sigma_z \simeq 0.003(1+z)$ proposed by the PAU Survey is close to optimal. Redshift space distortions and nonlinear effects can produce distortions that are comparable to this value, depending on what is the (biased) tracer that is used to measure BAO.

2.4. Estimating the BAO Scale

Armed with the conclusions from the previous discussion about photo- z errors and other nonlinear effects (clustering, bias, and redshift distortions), we are now in a position to give an estimate of the expected 1σ error determination from a survey with the characteristics of PAU. To this end, we will employ the two-point statistics in Fourier space (i.e., the power spectrum $P(k)$).

To estimate the error in the measurement of the power spectrum we will resort to the commonly used expression:

$$\sigma_P \equiv \frac{\Delta P(k)}{P(k)} \simeq \sqrt{\frac{2}{N_m(k)}} \left(1 + \frac{1}{\bar{n} P(k)} \right), \quad (9)$$

which can be derived from Feldman et al. (1994; see, for instance, Martínez & Saar 2002, Section 8.2), where $N_m(k)$ is the number of Fourier modes present in a spherical shell extending from k to $k + \Delta k$. In terms of the survey volume V , we have $N_m(k) = V(4\pi k^2 \Delta k)/(2\pi)^3$. The first term in Equation (9) corresponds to the sampling error and is independent of redshift. The second term corresponds to Poisson shot noise and \bar{n} denotes the number density of observed galaxies in the survey. This formula is exact when the probability

Table 2
Details of the Surveys Considered in Figure 18

Survey	z Range	Number Galaxies	Tracer	Area (deg ²)	Volume (Gpc ³ h ⁻³)	Radial Information	Timescale	Reference
WiggleZ	0.3 < z < 1.2	2.8×10^5	ELG	1,000	2.04	Yes	2007–2009	Glazebrook et al. (2007)
BOSS-LRG	0.2 < z < 0.8	1.5×10^6	LRG	10,000	8.06	Yes	2009–2014	See text
HETDEX	1.8 < z < 3.7	1.0×10^6	LAE	200	1.91	Yes	?	Hill et al. (2004)
WFOS-ELG	0.5 < z < 1.3	2.0×10^6	ELG	2,000	4.47	Yes	?	See text
WFOS-LBG	2.3 < z < 3.3	6.0×10^5	LBG	300	1.53	Yes	?	See text
PS1	0.3 < z < 1.5	5.0×10^8	ALL	20,000	65.3	No	?	
DES	0.3 < z < 1.5	1.5×10^8	ALL	5,000	16.3	No	2011–2015	
PAU-LRG	0.1 < z < 0.9	1.3×10^7	LRG	8,000	8.6	Yes	2011–2015	This paper

density function of spectral amplitudes is Gaussian and a very good approximation when the shot-noise term is negligible (see Angulo et al. 2008).

For $k \leq 0.12 h^{-1} \text{ Mpc}$ and for halos that host LRGs we expect that $P(k) > 2 \times 10^4 h^{-3} \text{ Mpc}^3$ ($b \simeq 2$) at $z \sim 0$. This agrees well with actual measurements of $P(k)$ for LRGs in the Sloan Digital Sky Survey (SDSS) catalog (see e.g., Figure 4 in Tegmark et al. 2006). As we will show below, the PAU number density of LRGs is expected to be $\bar{n} > 0.001 h^3 \text{ Mpc}^{-3}$ for $z < 0.9$, which implies that the Poisson shot-noise contribution to the error in Equation (9) is smaller than 8% at $z \sim 0.5$, even taking into account the degradation from a photo- z error of $\sigma_z = 0.003$ as discussed before.

The bump in the spatial correlation function translates into the power spectrum as a series of damped oscillations of a few percent in relative amplitude. This is shown in Figure 4 that contains the power spectrum of DM (left panel) and halos of mass $M > 4.7 \times 10^{12} h^{-1} M_\odot$ (right panel) measured in the MICE1536 simulation. In both panels the measured spectra have been divided by a smoothed one with the same broad-band power obtained from the data themselves (Percival et al. 2007b; Angulo et al. 2008). The solid red lines in Figure 4 show that this ratio can be roughly modeled as

$$\hat{P}(k) \simeq 1 + Ak \exp[-(k/0.1 h \text{ Mpc}^{-1})^2] \sin(r_{\text{BAO}}k), \quad (10)$$

which illustrates how $P(k)$ depends on the BAO scale.

Moreover, the discussion in Section 2.3 that led to Figure 3 validates to a good extent that photo- z , clustering, bias, and redshift distortions can be modeled in the power spectrum monopole as the angle average of

$$P(k, \mu) = b^2 P_{nl}(k)(1 + \beta \mu^2)^2 \exp[-k^2 \Delta^2 \mu^2], \quad (11)$$

where $\Delta = \sigma(1+z)/H(z)$ and $\sigma = \sqrt{\sigma_z^2 + \sigma_p^2}/2$. Therefore, except from nonlinear clustering, which is stronger than the intrinsic Silk damping of BAOs, and is responsible for the exponential damping in Equation (10), the remaining effects are multiplicative contributions to the measured $P(k)$, and they factor out when constructing \hat{P} . This means that the above described systematic effects do not affect the BAO signal in the spherically averaged $P(k)$, although they do increase the associated errors as we will discuss below. Thus, Equation (10) allows us to compute how the measured \hat{P} varies with the BAO scale,

$$d\hat{P}/dr_{\text{BAO}} \simeq Ak^2 \exp[-(k/0.1 h \text{ Mpc}^{-1})^2] \cos(r_{\text{BAO}}k). \quad (12)$$

Such a variation in \hat{P} produces a shift in the χ^2 fitting to measurements of $\hat{P}(k_i)$ given by

$$\Delta\chi^2 \simeq \sum_i \frac{\Delta\hat{P}^2(k_i)}{\sigma_P^2(k_i)} \simeq \Delta_{\text{BAO}}^2 \left(\frac{A}{r_{\text{BAO}}}\right)^2 \left(\frac{V}{r_{\text{BAO}}^3}\right) I^2[m],$$

where

$$I^2[m] = \frac{1}{(2\pi)^2} \int_0^{2\pi m} x^6 \frac{\exp[-2(x/10.86)^2] \cos^2(x)}{(1 + 1/\bar{n}P)^2} dx, \quad (13)$$

m is the number of BAO oscillations included in the fit ($k_{\text{max}} = 2\pi m/r_{\text{BAO}}$) and $\Delta_{\text{BAO}} \equiv \Delta r_{\text{BAO}}/r_{\text{BAO}}$. The shot-noise term includes the full power spectrum given by Equation (11) and accounts, in particular, for photo- z errors. In deriving Equation (13) we have explicitly used that for our reference cosmology $r_{\text{BAO}} = 108.6 h^{-1} \text{ Mpc}$.

A 1σ determination of Δ_{BAO} alone corresponds to $\Delta\chi^2 = 1$, so that

$$\Delta_{\text{BAO}}|_{\Delta\chi^2=1} = \left(\frac{r_{\text{BAO}}^3}{V}\right)^{1/2} \frac{1}{I[m](A/r_{\text{BAO}})}. \quad (14)$$

From Figure 4 we find that $A/r_{\text{BAO}} \sim 0.02$ fits well both halos and DM clustering. We then assume $m \simeq 2.5$ which corresponds to the range $0 < k < 0.14 h \text{ Mpc}^{-1}$ (including two BAO peaks) and obtain from Equation (14),

$$\Delta_{\text{BAO}} \simeq 0.33 \left(\frac{r_{\text{BAO}}^3}{V}\right)^{1/2} \simeq 0.33\% \sqrt{13 h^{-3} \text{ Gpc}^3 / V} \quad (15)$$

when we neglect completely the shot-noise term in Equation (11). Including the shot noise but no photo- z degradation yields a prefactor of 0.35% (for $\sigma_p = 400 \text{ km s}^{-1}$). If we also add a photo- z error of $\sigma_z = 0.003$ (as PAU) we find 0.36%. If instead, we add a photo- z error of $\sigma_z = 0.03$, the amplitude rises to 2.2%. In other words, we expect PAU to yield a measurement of BAO with only a 10% degradation with respect to an ideal survey, whereas a survey with an order-of-magnitude larger photo- z is expected to produce a factor of ~ 6.5 worse measurement. According to this, in a three-dimensional analysis, the relative error in the BAO scale is just approximately equal to the inverse of the square root of the number of independent regions of size r_{BAO}^3 that are sampled by our survey, and it is quite robust in front of close-to-optimal (PAU-like) photo- z error and nonlinear effects. For $V \simeq 10 h^{-3} \text{ Gpc}^3$ we get about $\Delta_{\text{BAO}} \simeq 0.5\%$. The above estimate is in good agreement with Table 2 in Angulo et al. (2008) and with the analysis in Blake & Glazebrook (2003) and Seo & Eisenstein (2003).

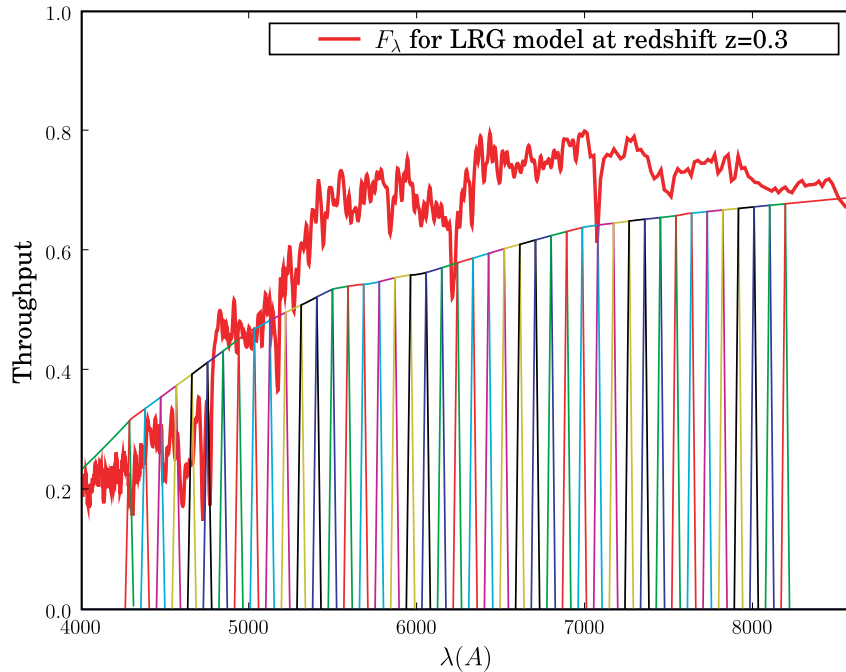


Figure 5. Example of a filter system similar to the one which will be used by the PAU Survey. We have included the redshifted spectrum of an early-type galaxy at $z = 0.2$ from the Bruzual and Charlot library to illustrate how the sharp 4000 \AA break (which here falls at 4800 \AA) is basically bracketed by only two filters. Note that the filters are spaced 93 \AA but have FWHM widths of 118 \AA due to the wavelength extent of their wings. The blue squares represent the flux which would be observed through the filters. Note that many spectral features apart from the 4000 \AA break are resolved by such a filter system.

(A color version of this figure is available in the online journal.)

If we limit ourselves to optical surveys of LRGs, we have $z \lesssim 1$. To get to $V \simeq 10 h^{-3} \text{ Gpc}^3$ we will have to map of the order of 8000 deg^2 . There are roughly two million LRGs with luminosity L above the characteristic galaxy luminosity L^* in 1000 deg^2 at $z < 0.9$ with magnitude $I_{AB} < 22.5$ (Brown et al. 2007). However, not all galaxies in a given volume need to be measured as long as $\bar{n}P > 3$, so that shot noise is subdominant in Equation (9). We will show below that it is in fact possible to get to $\bar{n}P \gtrsim 10$ with the subsample of PAU LRGs that have good quality redshifts.

3. SURVEY SIMULATIONS

The main distinctive feature of our survey is the use of photometric information to achieve the highly accurate redshift measurements needed to characterize the line-of-sight BAO signature. Since such an observational program has not been attempted before, we need to prove, at least conceptually, that it is possible to achieve precisions of $\sigma_z/(1+z) \simeq 0.003$ with photometric data. According to Section 2 and particularly Equation (9), we only need to reach such a precision for a galaxy population tracer with a space number density which satisfies $\bar{n}P(k) \gtrsim 3$. Ideally we would like galaxies that are luminous so we can observe them up to high redshift and that present a spectral energy distribution with distinctive features to achieve accurate photometric redshifts. The most luminous of the early-type galaxies (LRGs) constitute such a population. Their space number density is high enough. They are highly biased and they feature a prominent 4000 \AA break in their spectrum which, together with other spectral features, makes possible a precise estimation of their redshifts using photometric measurements (Figure 5). As a matter of fact, bright early-type galaxies were the subject of the first attempt to estimate photometric redshifts in the seminal paper of Baum (1962).

Hickson et al. (1994) was the first to propose using intermediate-band filters as a viable alternative to traditional spectroscopy. The COMBO-17 Survey (Wolf et al. 2001, 2003) puts this idea into practice, using a combination of traditional broad-band and medium-band filters. COMBO-17 reaches an accuracy of $\sigma_z \sim 0.02(1+z)$ for the general galaxy population (Hildebrandt et al. 2008), and has reached a scatter of $\sigma_z \sim 0.0063$ for the bright ellipticals in the Abell 901/902 superclusters. Taking into account the velocity dispersion of the cluster, the authors infer an intrinsic photometric accuracy close to $0.004(1+z)$ (Wolf et al. 2003).

Benítez et al. (2008) have shown that the most effective way of reaching high photo- z precisions is using a system of constant-width, contiguous, nonoverlapping filters. The ALHAMBRA Survey (Moles et al. 2005, 2008) has implemented such a filter system, and preliminary results for that survey show that it is possible to get close to $0.01(1+z)$ photo- z accuracy for the general galaxy population. LRGs usually have higher photo- z precisions than the rest of the galaxies (as it happens with the COMBO-17 data or the SDSS LRGs; Oyaizu et al. 2008; D'Abrusco et al. 2007), and it is expected that LRGs in the ALHAMBRA Survey will have photo- z errors substantially below $\sigma_z \sim 0.01(1+z)$.

In view of these results, it seems reasonable to suggest that a precision a few times smaller than $0.01(1+z)$ can be reached for the LRG population with filters that are 3 times narrower than those of ALHAMBRA, and about 2–3 times narrower than the medium-band filters in COMBO-17 (which do not fill the optical range contiguously). In what follows we try to demonstrate that the observing program required by PAU is feasible, and can deliver redshift values with $\sigma_z/(1+z) \simeq 0.003$ for LRGs.

In order to qualitatively understand the relationship between measurement uncertainties and the accuracy of the redshift estimation we can use a toy, step-like spectrum, flat in wavelength

except for a jump by a factor of D in the amplitude at 4000 \AA , i.e., we assume that the spectrum has a flux of F redward of the break and F/D blueward of it. This roughly approximates a low-resolution version of an LRG (Eisenstein et al. 2003). If we use a set of constant width, contiguous filters of width $\Delta\lambda$, the flux in the filter that spans the break will be equal to

$$f = \alpha \frac{F}{D} + (1 - \alpha)F, \quad (16)$$

where $\alpha = (\lambda_B - \lambda_0)/\Delta\lambda + 1/2 = Rz + k$, here $\lambda_B = 4000(1+z)$ is the observed wavelength of the break, λ_0 is the central wavelength of the filter, the ‘‘local resolution’’ is $R = 4000/\Delta\lambda$ and $k = (4000 - \lambda_0)/\Delta\lambda + 1/2$. We then have that

$$f = F[(D^{-1} - 1)(Rz + k) + 1] \quad (17)$$

and

$$z = \frac{1}{R} \left[\left(\frac{f}{F} - 1 \right) \left(\frac{D}{1 - D} \right) - k \right]. \quad (18)$$

The error in the redshift roughly depends on the flux measurement error σ_f as

$$\sigma_{z_f} \approx \frac{D}{R(D-1)} \frac{\sigma_f}{F}, \quad (19)$$

where we have considered that the error in the determination of F is much smaller than σ_f .

Apart from the photometric error, another source of uncertainty in the redshift estimation is the intrinsic variability of galaxy spectra around its average, even within such a homogeneous class as LRGs (Cool et al. 2006; Eisenstein et al. 2003). We can include this in our toy model as an uncertainty in the 4000 \AA break amplitude D . Using the above formulae we get that

$$\sigma_{z_D} \leq \frac{1}{R(D-1)^2} \sigma_D. \quad (20)$$

The total uncertainty predicted by the toy model is thus

$$\sigma_z \sim \frac{1}{R(D-1)^2} \sqrt{\sigma_D^2 + 2(\sigma_f/F)^2}. \quad (21)$$

We can estimate the intrinsic scatter in D to be $\sigma_D = 0.1$, as shown below. To check the validity of this formula we can use the photometric observations of LRGs with measured spectroscopic redshifts. We have downloaded an LRG catalog with spectroscopic redshifts from the SDSS Web site and estimated their photometric redshifts using the LRG template described below, measuring an average error of $\sigma_z \approx 0.02(1+z)$. Equation (21) clearly overestimates the error, since at e.g., $z = 0.3$, where galaxies have typically $\sigma_f/F = 0.05$, it would predict (using $D = 1.8$) an error from the template variability of $\sigma_{z_D} = 0.044$, a photometric error of $\sigma_{z_f} = 0.03$ and a total error of $\sigma_z = 0.05$, about twice as large as the real result $\sigma_z = 0.026$. This is not surprising, since real galaxies have many features which contain redshift information apart from the 4000 \AA break. Therefore, although Equation (21) can be useful to qualitatively understand the effects of intrinsic scatter and photometric noise on the photometric redshift accuracy, it clearly underestimates the precisions which can be achieved in practice.

The application of Equation (21) to our setup, with $\sigma_f/F = 0.1$ gives $\sigma_z = 0.006$, which again is twice what we expect. In what follows we will perform a detailed simulation to show that

it is feasible to reach the photometric redshift accuracy required for our experiment ($0.003(1+z)$) under realistic observing conditions, taking into account the shape of real galaxies, the behavior of the sky background as a function of wavelength and lunar phase, and the expected throughput and efficiency of astronomical instruments.

3.1. Observational Setup and Signal-to-Noise Ratio Considerations

In order to simulate the characteristics of the astronomical site where the PAU observations will be carried out, we assume that the sky brightness for the dark phase of the lunar cycle is similar to that of Paranal, as measured by Patat (2004). For the middle of the Moon cycle, or ‘‘gray’’ time we use the values of Walker (1987) for Cerro Tololo. Figure 6 shows the assumed sky brightness in the standard $UBVRI$ broad bands. However, due to the narrowness of our filters, it is necessary to have a good representation of the small-scale structure of the sky spectrum, for this we use the model optical spectrum of Puxley (2008), the same used for the Gemini exposure time calculator.

We have written an exposure time calculator for this task. To calculate the full throughput of the system we use the La Palma atmosphere at 1.2 airmass, two aluminum reflections, and the LBNL CCDs (Holland et al. 2003) quantum efficiency curves. We also approximate the throughput of the filter system using the values of the BARR filters produced for the ALHAMBRA Survey. The final result is shown in Figure 5. We match our results to those of the ING exposure time calculator, SIGNAL, using the same observational setup. To reproduce their results, which have been calibrated empirically, we have to degrade our theoretical estimates by 25%–10% (which are basically the values of the empirical corrections they use). We have checked our predictions with preliminary results from the ALHAMBRA Survey observations and they agree within 10%. We have compared the predictions of our simulator with those of the Direct Imaging Exposure Time calculator (DIET)¹⁹. DIET estimates 5σ point source limiting magnitudes of $g = 25.74$ (dark time) and $r = 24.94$, $i = 24.49$ (gray time) for 442 s exposures, within $\approx 1 \text{ arcsec}^2$ apertures and $0'.8$ seeing. We can scale these results taking into account the effective width of our narrow-band filters and the relative collecting mirror areas (10 m^2 for Canada–France–Hawaii Telescope (CFHT) versus $\pi \text{ m}^2$ for our fiducial telescope), corresponding to limiting magnitudes of $m_{F4982} = 23.63$, $m_{F6283} = 23.12$, and $m_{F7771} = 22.78$. Our predictions shown in Figure 7 are $m_{F4982} = 23.77$, $m_{F6283} = 22.98$, and $m_{F7771} = 23.15$. Most of the differences can be explained by the introduction by DIET of a coefficient which attempts to account for the incorrect measurement of the sky background for very small apertures and which worsens the signal-to-noise ratio (S/N) by a factor of 1.22 for faint objects.

The simulations below have been carried out assuming that the survey will use a dedicated 2 m class telescope, with an effective area of $\pi \text{ m}^2$, and a camera with a 6 deg^2 field of view (FOV). The results will remain qualitatively valid as long as the *etendue* of the final observational setup is roughly the same. Most likely the observations will be carried out in drift-scan mode. Since there is no need to change instruments, we expect that the observing efficiency will be very high and that only a maximum of the two CCD readouts per filter will be carried

¹⁹ <http://www.cfht.hawaii.edu/Instruments/Imaging/Megacam/dietmegacam.html>

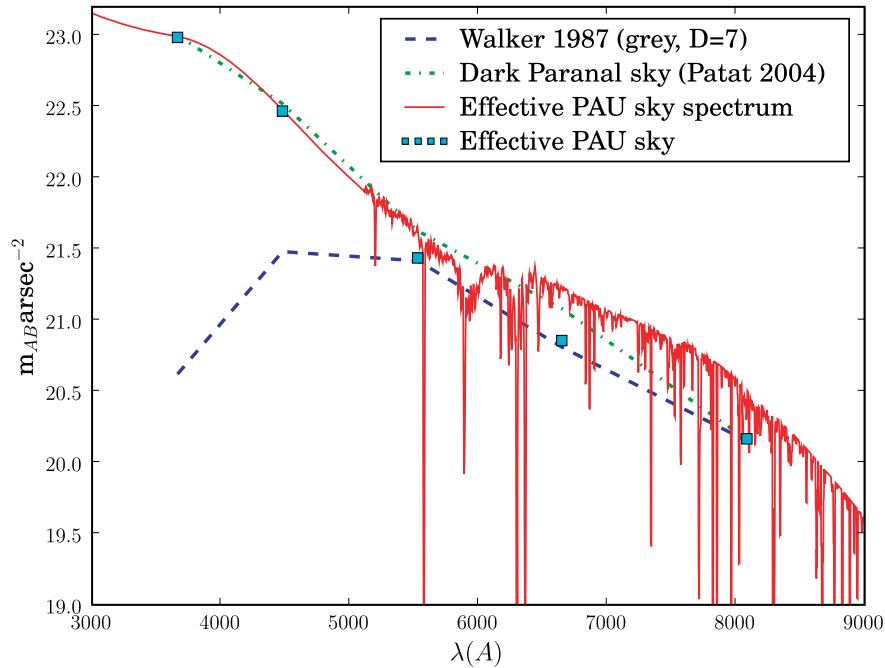


Figure 6. Sky background assumed for our simulations. We have assumed that we are able to adapt the choice of filters in our observations to the moon cycle, observing in the u band the darkest night, and then moving toward redder filters as the sky brightness grows. The red, continuous line corresponds to our expected “effective” sky spectrum, with the squares showing the equivalent broad-band AB magnitudes in the $UBVRI$ filters. The spectrum is normalized to have the same broad-band brightness as the Patat (2004) measurements of the dark sky at Paranal for the U and B bands, and the same as the middle of the cycle “gray” nights from Walker (1987) in the rest of the filters.

(A color version of this figure is available in the online journal.)

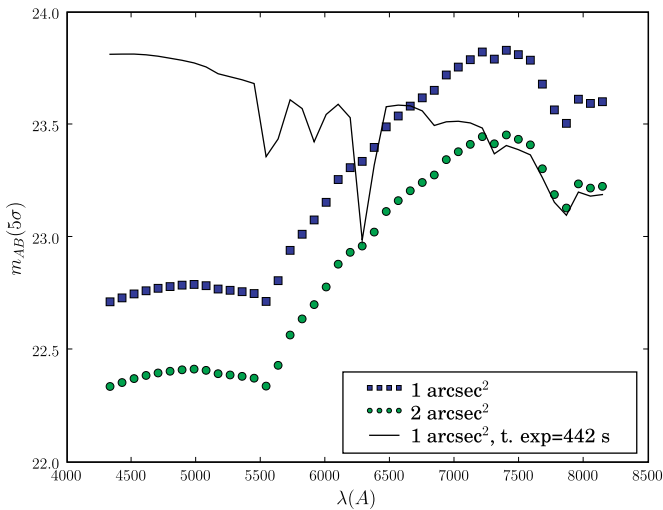


Figure 7. Expected limiting magnitudes for PAU-BAO. The squares represent the 5σ magnitude limits within a 1 square arcsec aperture, the circles within a 2 arcsec² aperture and the continuous line is the 5σ magnitude limit which would be reached if we divided the total exposure time of 19,440 s equally among all the filters.

(A color version of this figure is available in the online journal.)

out. Assuming that the useful time will be similar to that in Calar Alto (Sánchez et al. 2008) and that the moonlight will prevent us from taking data during three nights per Moon cycle, the number of useful hours per year amounts to 1930. Leaving some room for unforeseen incidences, we assume that the total number of hours of exposure time per year will amount to 1800. For a survey area of 8000 deg², and with a 6 deg² camera in a period of four years we expect to be able to expose each field a total of 5.4 hr, or 19,440 s.

The best way of measuring accurate colors for photo- z is using relatively small isophotal apertures (Benítez et al. 2004) which maximize the S/N of the color measurements, despite the fact that such an aperture leaves out a large amount of the flux, and they are therefore not optimal for other scientific purposes. In our S/N estimations we assume that we will use 2 arcsec² apertures, which enclose about 40% and 64% of the flux of respectively a $z = 0.2 L_*$ and a $z = 0.9 L_*$ galaxy. In the following subsection we explain how we calculate these corrections.

A crucial question is how to divide the exposure time between the different filters. At each redshift, we identify the filter which corresponds to the 4150 Å rest frame region, and try to detect an LRG L_* within a 2 arcsec² aperture at that redshift with at least a S/N of 10. We set a minimum exposure time of 120 s, and adjust the maximum exposure time in each filter so that the total is below 5.4 hr. The resulting exposure times are < 120 s for filters bluer than $F5446$, and increase until they reach the maximum exposure time of 861 s for $F7307$ and redder filters. The resulting 5σ limiting magnitudes are plotted in Figures 7 and 8.

3.2. Intrinsic Galaxy Variability

As Equation (21) shows, it is necessary to understand the intrinsic variability of LRGs in order to estimate the photometric redshift accuracy achievable with them. It is well known (Eisenstein et al. 2003; Cool et al. 2006 and references therein) that LRG galaxies (with $L > 2.2 L_*$) are a remarkably homogeneous class. At a fixed redshift, they form a red sequence, which varies slowly and regularly with absolute magnitude and environment. LRG galaxies in the red sequence present a scatter of only a few percent in the color defined by a pair of filters spanning the 4000 Å break. Therefore, if we know the absolute magnitude of an LRG and the richness of its environment, we

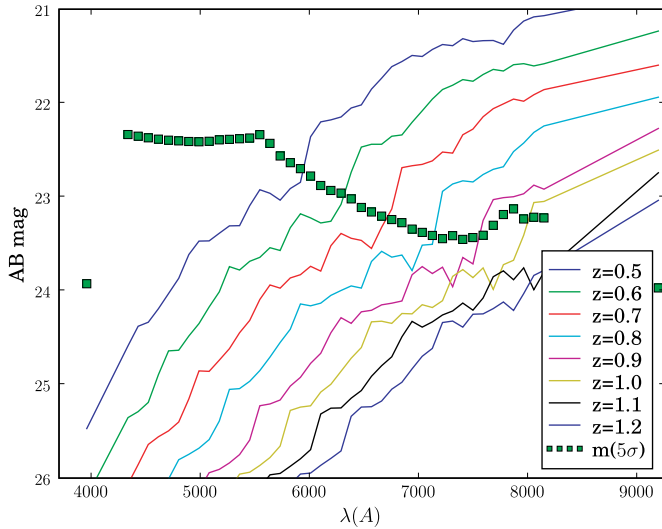


Figure 8. The expected 5σ limiting magnitudes for point sources (squares) and the observed spectra of a L_* red galaxy at different redshifts (without taking into account spectral evolution, but taking into account aperture corrections). Note that we are able to catch the rest frame 4000 \AA break with enough filters on both sides up to $z = 0.9$.

(A color version of this figure is available in the online journal.)

can predict its broad-band colors with a precision of at least $\sigma_{g-r} \approx 0.035$ (Cool et al. 2006).

It is not clear, however, which are the actual variations in the spectral shape of LRGs behind this broad-band scatter. The SDSS spectrophotometry is not good enough to accurately characterize this phenomenon, since its precision (about 0.05 mag in $g - r$ colors, according to the SDSS Web site and Adelman-McCarthy et al. 2008) is of the same order or even larger than the intrinsic color variation of real galaxies. In addition, the errors in the spectrophotometry are bound to be highly correlated and will be much worse at certain wavelength regions, like sky lines. The section of the SDSS Web site that describes the quality of the spectrophotometric calibration shows that below 4000 \AA the flux calibration error can be as large as 10%.

Since it is not feasible to use the SDSS spectral information, we have therefore decided to use a different approach to characterize this intrinsic spectral variability. Eisenstein et al. (2003) split the spectra of LRG into different classes and samples, and looked at the differences among them using Principal Component Analysis (PCA). They showed that most of the variation between these average classes can be ascribed to a single spectral component. It is therefore reasonable to assume that the intrinsic variation for galaxies of each class, responsible for the red sequence scatter described above, can be modeled approximately using the same PCA component. We have therefore generated a mock galaxy sample with $L > L_*$ at $z = 0.16$ using the red sequence described by Cool et al. (2006), and the luminosity function described in Brown et al. (2007), and fit their $g - r$ and $r - i$ colors using the average template of Eisenstein et al. (2003) and the first PCA component (shown in Figure 8 of Eisenstein’s paper).

The reason to limit ourselves to those two filters is that Eisenstein et al. (2003) only provide spectra in the $3650\text{--}7000 \text{ \AA}$ wavelength range, which does not include other filters. The comparison with the average Cool et al. (2006) colors show that we have to slightly correct Eisenstein’s average template to adapt it to the observations, subtracting the first PCA

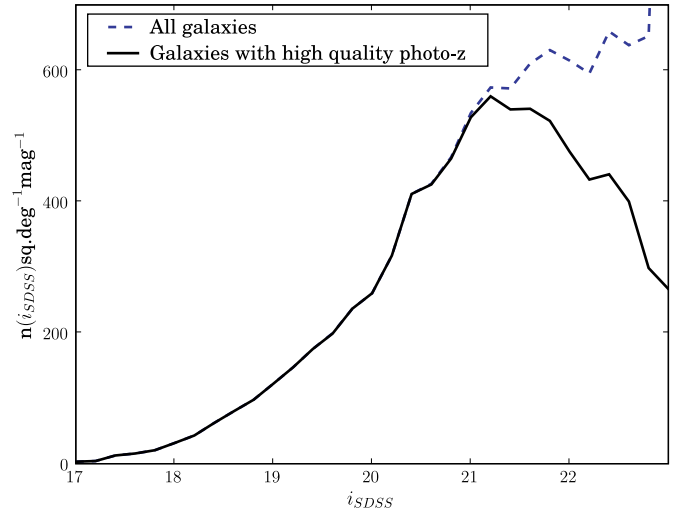


Figure 9. Differential number counts distribution of $L > L_*$ red galaxies. (A color version of this figure is available in the online journal.)

component multiplied by 1.74, and that the required variation of the amplitude of the PCA component needed to explain the intrinsic scatter around the red sequence is approximately 1.8 times that necessary to explain the variation of LRGs with redshift, magnitude, and environment. The average D4000 is 1.81, and the rms around this average value is 0.104. Therefore, the 4000 \AA break amplitude seems to display an intrinsic scatter of 6% in real galaxies.

3.3. Input Early-Type Catalog

To describe the early-type galaxy population we use the luminosity functions described in Brown et al. (2007). We populate a 10 deg^2 area with galaxies following this distribution and exclude those which are fainter than L_* (although it is obvious that many of them will be detected as well) and fainter than $I_{AB} = 23$.

LRGs are extended objects, and we have to calculate which is the fraction of the total flux that falls within our reference 2 arcsec^2 aperture. For this we use the data on galaxy sizes and their evolution provided by Brown et al. (2007), assuming, as they do, that galaxies can be well represented by a de Vaucouleur profile. The correction ranges from 1.5 mag at $z = 0.1$ to ≈ 0.5 for $z > 0.7$. The resulting differential numbers counts and redshift distribution are plotted with dashed lines in Figures 9 and 10 (note that we plot the magnitudes corresponding to a 2 arcsec^2 aperture).

3.4. Results

To simulate our observations we will redshift and integrate under the corresponding filter transmissions a spectrum resembling a typical LRG galaxy, and then try to recover its redshift using a Bayesian photometric redshift method (BPZ, described in Benítez 2000). Obviously in the real world we will not use a single template for all LRGs between $0 < z < 0.9$: their spectra are known to vary with redshift and luminosity (Eisenstein et al. 2003; Cool et al. 2006). However, as that paper shows, the variation is smooth and easy to parametrize. This is confirmed by *Hubble Space Telescope* (HST) very deep observations of galaxy clusters, where the scatter around the red sequence remains small (~ 0.03) up to $z = 1$ and higher (Blakeslee et al. 2003).

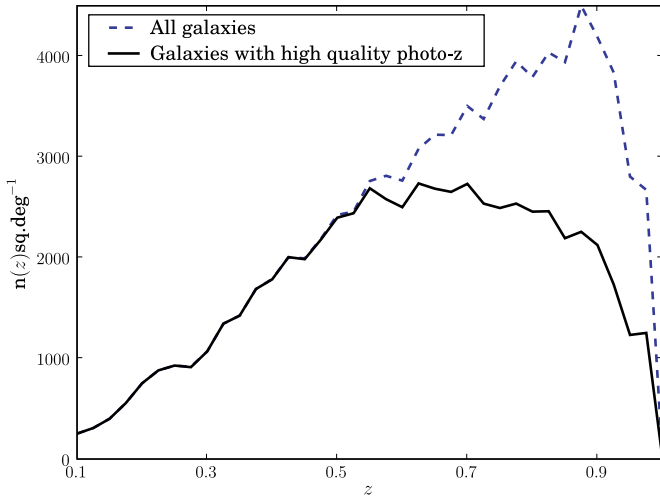


Figure 10. Redshift distribution of $L > L_*$ red galaxies. (A color version of this figure is available in the online journal.)

We assume that we will be able to split our LRGs into subsamples such that for each of them we can define an empirically calibrated template (using a technique similar to that of Budavári et al. 2000 or Benítez et al. 2004) which correctly represents the average galaxy colors for that galaxy subsample. Using standard photo- z techniques (Benítez 2000) we reasonably expect to be able to determine the redshift and spectral type of our galaxies in a preliminary pass to within $0.01(1+z)$. This is already being done for the ALHAMBRA Survey (Benítez et al. 2008; Moles et al. 2008). Thus, for each galaxy we will have a preliminary estimate of its redshift to within $\sigma_z \sim 0.01(1+z)$ and its absolute magnitude to within $\sigma_M \sim 0.15$ (within the redshift interval $z < 0.9$). This ensures that we can pin down the required template for each galaxy with large certainty (the error in the absolute magnitude corresponds to an intrinsic color variation of only 0.004 mag, much smaller than the expected scatter around the sequence at each redshift, 0.03–0.04 mag).

The LRG template corresponds to $z < 0.5$ galaxies, and one may wonder if the results obtained with this template are representative of higher redshift LRGs. Homeier et al. (2006) have measured the $V_{606} - I_{814}$ colors of a pair of clusters at $z = 0.9$ with the Advanced Camera for Surveys aboard *HST*. They measure a red sequence that is only 0.09 bluer than the colors predicted by our LRG template which illustrates the small amount of color evolution expected to $z < 1$ and shows that the results obtained with our LRG template should be similar to those obtained with real LRG templates at higher redshifts.

In our simulation we generate the galaxy colors using a combination of the average Eisenstein et al. (2003) template, corrected as mentioned above and the first PCA component, multiplied by a coefficient with a Gaussian distribution of rms = 1.8. This first PCA component scatter represents well the real broad-band scatter of galaxies observed by Cool et al. (2006) for $L > 2.2 L_*$ LRGs. We extrapolate this scatter to $L > L_*$. We also add a 2% noise to represent the expected scatter in the zero-point determination across the survey.

Then we calculate photometric redshifts using the Bayesian photometric redshift method implemented in the BPZ code and a single LRG reference template. We have also tried a template library with 11 templates, formed by linear combinations of the LRG template and the first PCA component encompassing $\pm 3\sigma$

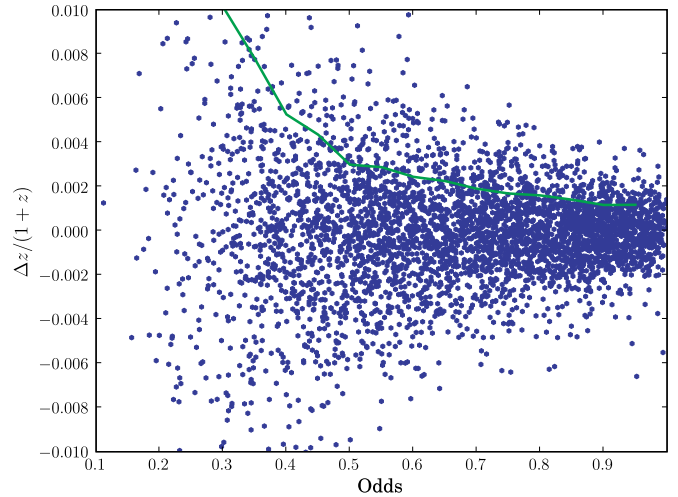


Figure 11. Photometric redshift error as a function of the Bayesian odds. Note that a cut at odds = 0.55 eliminates most of the objects with high redshift errors. For the sake of clarity, only one in every five points is plotted. The solid line corresponds to the rms of $\Delta z/(1+z)$ for each value of the odds.

(A color version of this figure is available in the online journal.)

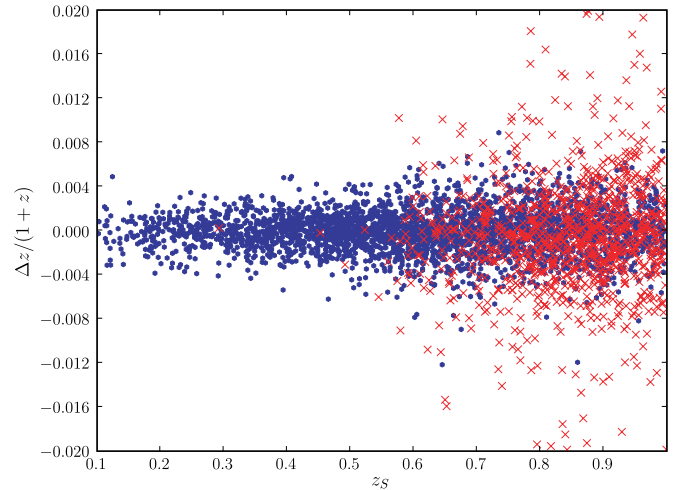


Figure 12. Scatter plot comparing the normalized difference between the photometric redshifts and the “true” input redshifts z_s . The red points are eliminated by the odds < 0.55 cut. For the sake of clarity, only one in every five points is plotted.

(A color version of this figure is available in the online journal.)

variations and the results are basically the same. For simplicity we quote the results obtained with only one LRG template.

With a single template, there is no point in using a prior, but the Bayesian framework still remains useful: it produces the so-called “odds” parameter, a highly reliable quality indicator for the redshift estimate. In Figure 11 we plot the scatter diagram corresponding to the quantity $(z_{\text{phot}} - z_s)/(1+z_s)$, where z_s is the true redshift, as a function of the odds parameter, together with the rms corresponding to each value of the odds. We can see that if we exclude the objects with low values of the odds parameter we get rid of most of the redshift outliers. The effectiveness of this technique has been often validated with real data (Benítez 2000; Benítez et al. 2004; Coe et al. 2006). Note that using a cut in χ^2 does not work well to eliminate outliers, as was shown by Benítez (2000).

We thus proceed to eliminate the objects with odds < 0.55 from our catalog. Figure 12 shows the scatter diagram for

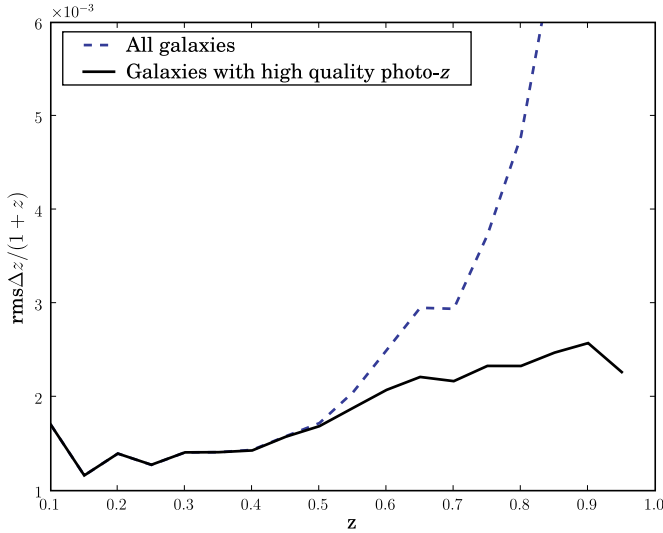


Figure 13. Photometric redshift error as a function of redshift, for all $L > L_*$, $I < 23$ red galaxies, and for the subset with high-quality photo- z . (A color version of this figure is available in the online journal.)

$(z_{\text{phot}} - z_s)/(1 + z_s)$ now as a function of the real redshift, z_s . Once the odds cut is applied there are no large outliers.

The resulting redshift and number counts distributions are plotted as solid lines in Figures 9 and 10. In Figure 13 we plot the resulting accuracy as a function of redshift. We are safely below the $0.003(1+z)$ limit for all our redshift range. Finally, in Figure 14 we plot the number density of all the galaxies, and of those with high-quality photo- z as a function of redshift. These figures show that we have a spatial density of $\bar{n} > 10^{-3} h^3 \text{Mpc}^{-3}$ in the redshift range $z < 0.9$. Since $P(k) > 10^4 \text{Mpc}^3 h^{-3}$ for LRGs (see e.g., Figure 4 in Tegmark et al. 2006) and $k < 0.2 h \text{Mpc}^{-1}$, we will have $\bar{n}P(k) > 10$ for the k range of interest for BAO, so that, according to Equation (9), shot noise will be negligible.

Finally, there are two caveats to consider. First, there are no spectroscopic data with good enough spectrophotometric calibration for LRGs in the redshift range of interest. We can therefore only estimate the intrinsic variation of the galaxies from the data available. We have assumed that it will behave similarly to the variation among LRG types described by Eisenstein et al. (2003). Second, the PCA study only covers the 3650–7000 Å range, and we assume that there is no template variation outside this range. We feel that this is justified since most of the redshift information for the galaxies is in practice contained in this interval, especially at high redshift.

3.5. Comparison with a Spectroscopic Survey

A typical multifiber spectroscopic survey with about 1000 fibers and a resolution $R \sim 2000$ in a telescope similar to the one we are assuming here (2 m class, about 6 deg² FOV, etc.) will reach up to a magnitude $i < 20$ in about 2 hr long exposures (BOSS 2008), assuming the transmission of a good optical spectrograph and low readout noise. This allows covering in a year close to 4000 deg² with $0.1 < z < 0.8$ for LRGs, or about $2.5 \text{Gpc}^3 h^{-3}$ per year. In our PAU approach, with our 300–900 s (depending on the band) exposures, we can cover about 2000 deg² per year with $0.1 < z < 0.9$ for LRGs, which translates to about $2 \text{Gpc}^3 h^{-3}$ per year, however with higher galaxy density. This results in $\bar{n}P(k) > 10$ at the relevant scales (see Equation (9)), while for a spectroscopic survey similar to

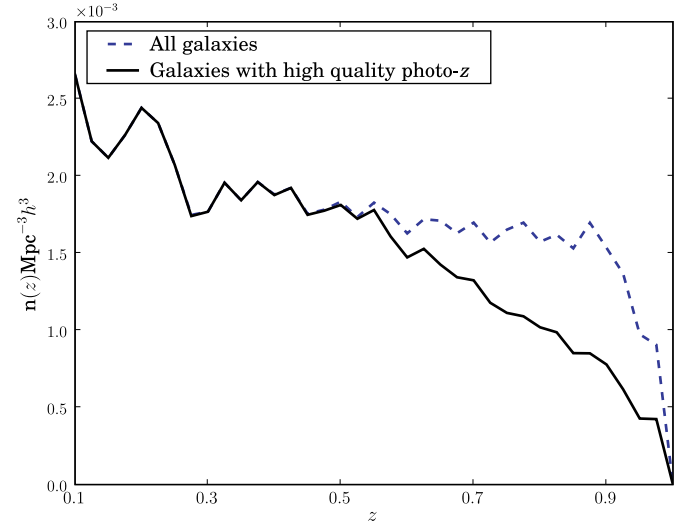


Figure 14. Spatial density as a function of redshift, for all $L > L_*$, $I < 23$ red galaxies, and for the subset with high-quality photo- z . (A color version of this figure is available in the online journal.)

BOSS (2008), with about 1000 fibers in a 6 deg² FOV, one can only reach $\bar{n}P(k) \sim 1$. Putting volume per year and galaxy density together, for an equal-time survey one gets

$$\frac{(\Delta P/P)_{\text{PAU-BAO}}}{(\Delta P/P)_{\text{spect}}} = \sqrt{\frac{2.5}{2}} \frac{1 + 1/10}{1 + 1/1} \sim 0.6. \quad (22)$$

For the radial modes, one further needs to take into account the slight degradation in information that affects the PAU measurement with its $\sigma(z) = 0.003(1+z)$.

Furthermore, in the imaging survey one gets many more galaxies than the LRGs. A preliminary study for the whole galaxy population obtains a good photometric redshift determination, $\sigma(z) \approx 0.01(1+z)$, for a large number of them (over 200 million). These galaxies would deliver a constraint on the BAO scale of similar power than the one from LRGs (although correlated, since both galaxy distributions trace the same underlying density fluctuations), so that the combination of both would improve the sensitivity, and could serve as a cross-check on systematic errors.

3.6. Calibration Requirements

We present here some general considerations to give an idea of what level of photometric and spectroscopic calibration is required to measure the BAO scale with PAU. In the following section we will address the issue of whether these requirements can be met in practice. We split this section into photometric and photo- z requirements.

3.6.1. Photometric Calibration

The magnitude of a galaxy that we measure in the survey, m_O , is the sum of the true magnitude m , plus a random statistical error that arises from photon and detector noise, e_{mr} , plus a systematic error e_{ms} . The systematic error arises from a variety of effects. For example, variations across the survey of the exposure time, mean atmospheric absorption, and sky background; nonuniformity of galactic dust absorption and inaccuracies in its correction; variations in the instrument/detector efficiencies through the duration of the survey. All these effects are assumed to have been corrected for through

calibrations with standard stars and flat fielding corrections. But inevitably, every correction has an error which contributes to e_{ms} . While the random statistical errors of any two galaxies are uncorrelated, the systematic errors in the magnitude over the survey have a correlation function $\xi_{ms}(z, \theta, g)$ that is likely to depend on redshift and angular separation θ , as well as galaxy properties g (e.g., luminosity, morphology, or color).

The random statistical errors have an effect that is reduced as the number of galaxies is increased. Generally the galaxy number shot noise will be larger than the error introduced by random errors in the apparent magnitude, as long as these magnitude errors are not very large. So if the number of galaxies that is observed is large enough the statistical errors should be small compared to the uncertainty in the correlation function due to cosmic variance. The systematic errors, however, do not go down with the number of galaxies observed.

For a flux-limited survey, a magnitude calibration covariance across the sky $\Delta_m(\theta)$ will result in angular density fluctuations $\delta(\theta)$. If we take the number of galaxies brighter than magnitude m to be $N(< m) \simeq 10^{\alpha m}$ (typically $\alpha \ln 10 \simeq 1$), then a magnitude error translates into a number density fluctuation error:

$$\delta \simeq \alpha \ln 10 \Delta_m. \quad (23)$$

We can decompose the calibration error field in the sky into spherical harmonics. We would like the resulting spectrum of calibration errors C_l^m

$$C_l^m = 2\pi \int_{-1}^1 d \cos \theta \Delta_m(\theta) P_l(\cos \theta) \quad (24)$$

to produce errors in the angular power spectrum C_l which are smaller than the sampling variance errors in C_l :

$$C_l^m < \frac{\Delta C_l}{\alpha \ln 10} \simeq \frac{C_l}{\alpha \ln 10 \sqrt{f_{\text{sky}}(l+1/2)}}. \quad (25)$$

We will assume that angular clustering will be sampling variance rather than shot-noise variance dominated. We also assume Gaussian statistics. The corresponding errors in the correlation function $\Delta_m(\theta)$ are

$$\Delta_m(\theta) = \sum_l \frac{2l+1}{4\pi} C_l^m P_l(\cos \theta). \quad (26)$$

The BAO scale projects at angles between $3^\circ.7$ and $1^\circ.7$ for redshifts between $z = 0.4$ and $z = 1.0$ (smaller redshifts cover a negligible volume). Unfortunately, the FOV of the planned PAU camera plans to cover very similar angular scales. We therefore need to be careful about calibration on the FOV. At angular scales $3^\circ.7$ and $1^\circ.7$, the requirement in Equation (26) translates into rms correlated calibration errors smaller than 2%–3% (i.e., 0.02 and 0.03 rms magnitude errors) in units of $(b/2)/(\alpha \ln 10)$ for $f_{\text{sky}} = 0.2$. This is for the whole (flux-limited) sample (mean $z \simeq 0.7$). These constraints become looser when we split the sample into redshift bins because the amplitude of clustering increases as we reduce the projected volume. The detailed constraints are shown in Figure 15.

3.6.2. Selection Effects on $\xi_2(r)$

Another angle to look at possible photometric calibration effects is to assume that different systematics on the galaxy density fluctuations will act as multiplicative correction over the

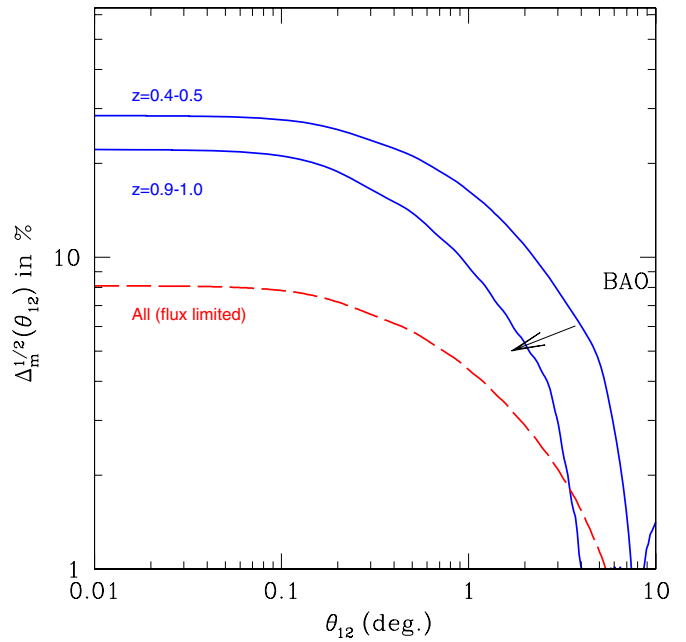


Figure 15. Required systematic calibration error (rms percentage) for two broad redshift slices (thick blue continuous lines): $z = 0.4\text{--}0.5$ (top) and $z = 0.9\text{--}1.0$ (bottom) and for a flux-limited sample (red dashed line) including all galaxies to the depth of PAU (mean $z = 0.7$). In these units, at BAO scales (which is a function of z and is marked by the arrow) the correlation in calibration error has to be smaller than about 6% for $z \simeq 0.45$ and 5% for $z \simeq 0.95$. For other science, the stronger requirements are driven by the flux-limited sample, i.e., $< 2\%$ and $< 8\%$ in correlated errors on scales smaller than 4° and $0^\circ.1$, respectively, as given by the dashed line.

(A color version of this figure is available in the online journal.)

galaxy density at a given position in the sample. We will assume that this type of error is uncorrelated to the galaxy clustering so that

$$\xi_{\text{obs}}(r) = \xi(r) + \xi_e(r), \quad (27)$$

where $\xi(r)$ is the true correlation and $\xi_e(r)$ is the correlation due to systematics in selection and calibration. To see how this could affect the BAO scale measurement we model the true correlation around the BAO scale as a Gaussian peak of width σ_0 . We further assume a generic power-law $\xi_e(r) \propto r^{-\beta}$ for the error around the BAO scale. The relative shift in the BAO scale can be found by Taylor expansion around the peak:

$$\Delta_{\text{BAO}} = \beta \frac{\xi_e(r_{\text{BAO}})\sigma_0^2}{\xi(r_{\text{BAO}})r_{\text{BAO}}^2}. \quad (28)$$

This requires an amplitude of $\xi_e(r_{\text{BAO}}) < 0.002$ if we want a shift in the peak $\Delta_{\text{BAO}} < 1\%$ and $\beta \simeq 2$. We have used here $\sigma_0 \simeq 15 \text{ Mpc } h^{-1}$, $r_{\text{BAO}} \simeq 100 \text{ Mpc } h^{-1}$, and $\xi(r_{\text{BAO}}) \simeq 0.01$ from Figure 3. This corresponds to a 20% error in the correlation at the BAO scale, and about $\sqrt{\langle \xi_e \rangle} = 4.5\%$ error on density fluctuations.

We have also tested the above calculations directly in simulations, by adding $\xi_e(r)$ and recovering the BAO scale.

Using Equation (23), this value of $\xi_e(r_{\text{BAO}}) < 0.002$ corresponds to $\Delta m < 0.05$ (in units of $\alpha \ln 10$ with $N(< m) \simeq 10^{\alpha m}$). Thus, with very different assumptions we reach the same conclusion on the requirement on photometric accuracy of around 5% on the BAO scale.

3.6.3. Photo- z Bias

Systematic errors in the radial direction (photo- z biases) also need to be under careful control. At any given redshift, we would like the mean in the photo- z measurements to differ from the true redshift by less than 1% (the target in Δ_{BAO} accuracy) in the radial BAO distance, i.e., $\sigma_r \simeq 1 \text{ Mpc } h^{-1}$, which corresponds to

$$\Delta_z = \sigma_r H(z)/c \simeq 5 \times 10^{-4} (z = 0.8), \quad (29)$$

where the numerical value corresponds to $z = 0.8$ and $\Omega_m = 0.2$. This is about an order of magnitude better than the statistical error at the same redshift, i.e., $\sigma_z \simeq 0.003(1+z) \simeq 5 \times 10^{-3}$.

Note that this is a conservative approach because we need the Δ_{BAO} accuracy as measured by galaxy density fluctuations and not by the absolute distances to the galaxies. The former will probably result into a weaker constraint for Δ_z .

3.7. Calibration Plan

As a summary for the above requirements, we need relative calibration to be better than about 3%–5% to avoid systematic effects on density fluctuations to dominate over intrinsic fluctuations on the BAO scale. On top of this we would like to have a bias in the photo- z scale to be below 1% on radial measurements of the BAO scale.

In terms of global photometry, it has now been shown that a homogeneous global relative calibration below 2%–3% accuracy is possible in current and future surveys (e.g., Sterken 2007 and references therein). The large FOV required by the PAU Survey and the drift scanning strategy will both help in the provision of standard calibration techniques, such as done in SDSS. We will also need to use a set of calibrated standard spectra of stars (or galaxies) to monitor and correct for relative color bias between narrow bands.

Apart from these “classical” techniques, it seems to be possible to use the observed colors of galaxies with spectroscopic redshifts as a photometric calibrator. In *HST*’s Ultra Deep Field, Coe et al. (2006) have been able to calibrate the NICMOS zero points using the comparison between predicted colors using the templates of Benítez et al. (2004) and ~ 50 spectroscopic redshifts. Similar techniques have been used for the COSMOS field (Capak et al. 2007) and are being applied to ALHAMBRA (Moles et al. 2008). Further work with the later survey will help refine our calibration redshift requirements.

Independently of the exact photo- z method finally used for the survey, it will be equivalent to defining a function $z = f(p, C, o)$, where p are a set of parameters describing the function, o are a set of observables such as the approximate redshift of the galaxy (determined with standard photo- z techniques), its luminosity, size or environment density, and C are the observed colors. The LRG population under study is relatively homogeneous and its changes with redshift and magnitude can be described with a very compact set of parameters (Eisenstein et al. 2003). If we determine the parameters p with enough precision to reach a redshift error σ_z over the whole range under consideration, then, provided that the parametrization is flexible enough to adapt itself to the observed redshift/color relationship of galaxies, the systematic zero-point error, averaged over all the galaxies, will be equivalent to $\sigma_z/\sqrt{N_c}$, where σ_z is the rms redshift error and N_c is the number of calibrators. We expect to have a calibration set with several thousand galaxies, easy to reach with 10 m telescopes as the GTC, and therefore will have negligible redshift bias.

4. THE SURVEY INSTRUMENT

The approach of the PAU project is to use known and proven technologies to build a large FOV camera and mount it on a telescope that is optimized for the survey.

The simulations presented in previous sections use a baseline concept of camera plus telescope with a large *etendue*, $A\Omega \approx 20 \text{ m}^2 \text{ deg}^2$. This *etendue* is achieved by means of a telescope with a 2 m effective aperture and a camera with 6 deg^2 FOV. A total of 42 filters is considered, each one having a width of 100 \AA in wavelength. The full filter system covers a range that goes from ~ 4000 to $\sim 8000 \text{ \AA}$, completed by two broad-band filters similar to the SDSS u and z bands.

In this section, we present the main ideas of a possible implementation of such a system. The goal is to show the feasibility of the telescope/camera system, and not to present a complete design.

4.1. Optics

Achieving a many filter, very large area survey in a relatively short time and the need for a rather large value of the *etendue* demand a very large FOV. The depth is not a major concern since the targets are bright galaxies in all the surveyed redshift range. Therefore, the FOV is the main driver of the optical design.

To give some quantitative estimates, with a telescope of 2.3 m aperture, a pixel size of $0''.4$ and state of the art detectors, it is possible to reach $S/N \sim 5$ for a star of $m(AB) = 23.5$ in $\sim 300 \text{ s}$ in all the spectral range bluer than 7500 \AA . Since the survey should cover, as argued before, an area of at least 8000 deg^2 , a FOV of 6 deg^2 is needed to be able to perform the survey in four to five years.

It is important to note that we do not intend to use detailed information on the morphology/shape of the objects, which relaxes the requirements on the image scale. This is the reason to choose a rather modest plate scale that translates $15 \mu\text{m}$ pixels into $26 \text{ arcsec mm}^{-1}$.

These FOV and plate scale are the basic requirements for a telescope that will be dedicated to the survey until its completion. These optical requirements for such a large FOV telescope and the corresponding panoramic CCD camera are demanding but they appear feasible.

The next optical elements are the filters. They are intended to have transmission curves with very sharp limits and minimal wavelength overlap, very similar to the filters in the ALHAMBRA Survey (Moles et al. 2005, 2008; Benítez et al. 2008) but 100 \AA wide.

The location of the filters in the path to the detectors can affect the final efficiency of the system. Two options are being considered: attaching the filters directly over the CCDs or on plate holders that could be interchanged. The first option is mechanically simpler but reduces the survey flexibility. The second one allows the optimization of the exposure times using different sets of filters depending on the moon-phase or any other external constraint, but its practical implementation is more demanding. The final decision will be taken when all the practical aspects of the survey, such as observing mode and calibration strategy, are fixed.

4.2. Focal-Plane and Observing Strategy

The baseline concept for the camera is a large mosaic of CCDs covering the 6 deg^2 FOV. The scientific goals can be reached with pixels of $0''.40$. Since most of the current

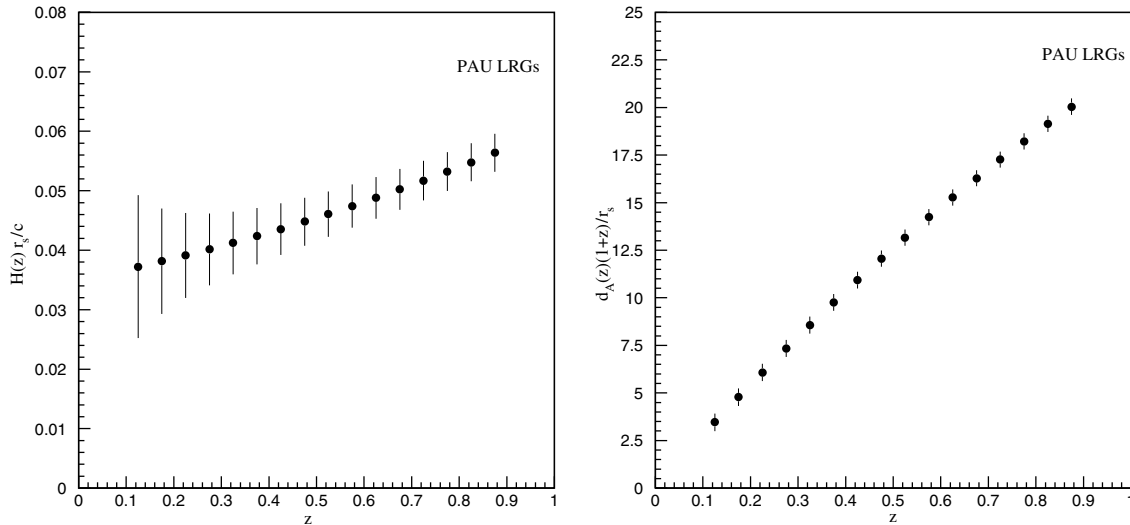


Figure 16. Left: the expected measurement of radial BAO scale from the PAU Survey (LRGs only). Right: same for the measurement of the transverse (angular) BAO scale.

(A color version of this figure is available in the online journal.)

astronomical large CCD detectors have pixel scales of $15 \mu\text{m}$, we need a camera of around 500 Mega-pixel or a number of $2\text{K} \times 4\text{K}$ CCDs that ranges in between 60 and 80, including a few CCDs for focusing and guiding purposes.

The baseline CCDs under consideration for the PAU camera are the fully depleted, high resistivity, $250 \mu\text{m}$ thick devices developed by the Lawrence Berkeley National Laboratory (LBNL; Holland et al. 2003). These CCDs ensure a very high quantum efficiency in the red zone of the wavelength region covered by PAU. However, the different possibilities of optimization have some impact in the focal plane instrumentation. There is the possibility of having two different types of CCDs covering different regions of the focal plane, in direct correlation with the filters, in order to maximize the sensitivity in the whole wavelength range. Thin blue-sensitive CCDs correlated with blue filters and thick red-optimized CCDs correlated with red filters. Several suppliers of CCDs are available for thin blue-optimized CCDs. A final decision for the focal plane instrumentation will be taken considering the global optimization of the survey.

The camera vessel will need to contain a liquid nitrogen reservoir to maintain the focal plane cold for several hours, ensuring stability and not compromising the efficiency of the observations. We will also investigate the choice of cryo-coolers or pulse tube coolers, taking into account the mechanical requirements that impose a stable precision of a few microns on the positioning of the CCDs in the focal plane.

The best observing strategy for a project of these characteristics is the time-delay-and-integrate (TDI) drift scanning mode. Drift scanning is a powerful imaging technique in which the telescope is kept stationary and one lets the sky image drift across the CCDs. Normally, TDI mode is operated at sidereal rate, and the lines of the CCD must be read in perfect synchronization with the movement of the sky at the focal plane. In this way, long continuous strips of the sky are imaged and large fields can be explored automatically, which makes this observing strategy particularly well suited for large surveys. Therefore, it is considered as the baseline strategy for PAU.

4.3. Front-End Electronics

The readout of a focal plane of the size of the PAU camera is a challenge. One of the most attractive options to read out such

a large number of CCDs is to use the open system MONSOON (Starr et al. 2004), developed by the instrumentation division of the National Optics Astronomical Observatory (NOAO), supported by the US NSF. A custom-made system or a commercial one, such as the Leach controller (Leach et al. 2000), is also being considered.

MONSOON is a generic readout system which consists in three kind of boards: the Acquisition Board, responsible for the bias voltage generation and the digitization of signals coming from the CCDs, the Clock Board, responsible of the clock signal generation needed to read out the CCD, and the Master Control Board, responsible of the event building and the data transmission to the DAQ computer. The system can be customized to meet the specific and demanding requirements of the PAU camera.

5. SCIENCE CAPABILITIES

5.1. The BAO Scale

We have performed extensive simulations of the PAU Survey, assuming 8000 deg^2 covered up to $z = 0.9$ using LRGs with the galaxy density given in Figure 14 and the redshift precision from Figure 13. This results in measurements of $H(z) \cdot r_s$ and $d_A(z)/r_s$, r_s being here the sound horizon at recombination, which are plotted in Figure 16. The relative precision achieved improves monotonically with increasing redshift, flattening out at about 5% for $H(z)$ and 2% for $d_A(z)$.

We have split the redshift interval from $z = 0.1$ to $z = 0.9$ into 16 equal bins. Results do not change if we change the binning. Combining these measurements into a cosmology fit, taking into account correlations, leads to determinations of the parameters Ω_m , w_0 , w_a . In the following, we will be using the standard parametrization (Chevallier & Polarski 2001; Linder 2003) of the time evolution of the DE equation of state, $w(z) = w_0 + w_a \cdot (1 - a)$, where w_0 denotes the equation of state now, and w_a is (minus) its current derivative with respect to the scale factor a . The value of the reduced Hubble constant, h drops out of the measured quantities. The left panel of Figure 17 shows the 68% confidence level (CL) contour in the $\Omega_m - w$ plane that can be achieved using only PAU LRG data. The corresponding 1σ errors are $\sigma(\Omega_m, w) = (0.016, 0.115)$. A flat universe and

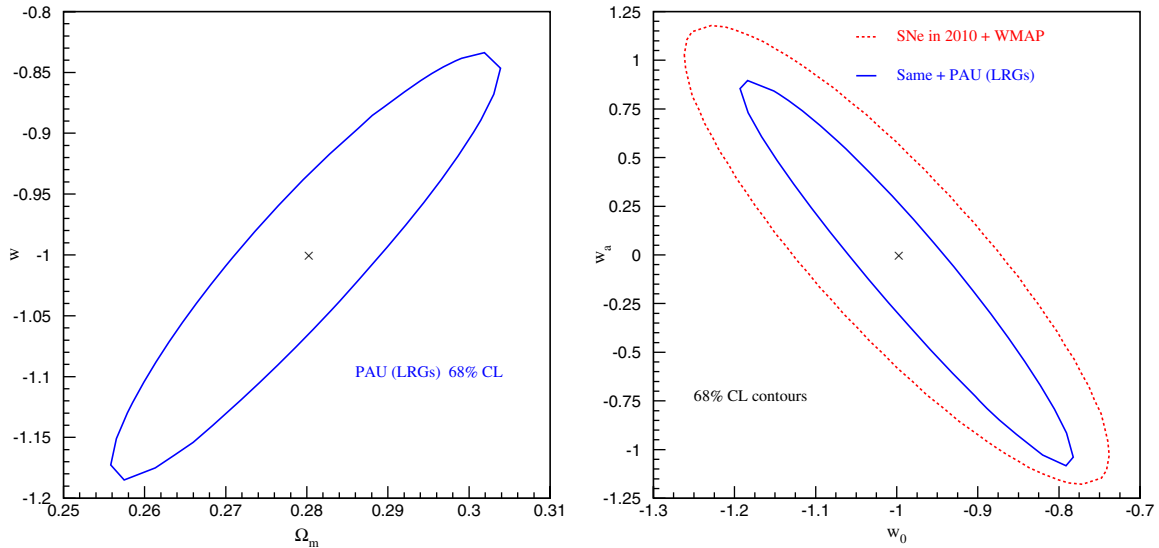


Figure 17. Left: 68% confidence-level contours in the Ω_m - w plane, using only PAU data, assuming a flat universe and a constant equation of state w . Right: 68% confidence-level contours in the w_0 - w_a plane for the world combined data from SNe and *WMAP* in about 2010, and after adding PAU data to that data set. The area of the contour decreases by about a factor of 3. A flat universe has been assumed.

(A color version of this figure is available in the online journal.)

constant equation of state has been assumed. In the right panel of Figure 17, 68% CL contours are shown in the w_0 - w_a plane, assuming a flat universe. The outermost contour approximates the expected world-combined precision from supernovae (SNe) and *WMAP* when PAU will start taking data, while the inner contour adds the PAU LRG data to the previous data set. The reduction in area corresponds to an improvement by more than a factor of 3 in the DETF figure of merit. The 1σ errors are $\sigma(w_0, w_a) = (0.14, 0.67)$.

We have also simulated a straw-man spectroscopic survey with equal area and depth but with $\sigma_z = 0.0005(1+z)$. The greatly improved redshift precision results in only a modest 20% decrease in the cosmological parameter uncertainties. Actually, the larger galaxy density that a photometric survey affords overcompensates for this deficit, as can be seen in Figure 18, where our simulated reach for several proposed BAO Surveys is compared. Details of the survey characteristics are taken from public sources and are summarized in Table 2. For Wiggle-Z, we adopt the total number of galaxies and redshift distribution as given in Glazebrook et al. (2007). Surprisingly, our Wiggle-Z constraints on DE parameters are approximately a factor of 2 worse than what one would predict from the errors on the d_A and H measurements quoted by the authors. We use the information in Section 3 of the SDSS3 project description (<http://www.sdss3.org/collaboration/description.pdf>) to simulate BOSS. The information for HETDEX is taken from Hill et al. (2004). The WFMOS Surveys details are taken from the Feasibility Study Report, which can be found at <http://www.gemini.edu/files/docman/science/aspens/>. The Pan-STARRS 1 Survey (PS1) and Dark Energy Survey (DES) information are taken from their Web pages (<http://pan-starrs.ifa.hawaii.edu/> and <http://www.darkenergysurvey.org/>).

5.2. Other Probes of DE

5.2.1. The Galaxy Clustering in Redshift Space

The redshift accuracy will be sufficiently good to identify individual structures (walls and voids) along the line of sight (see Figure 2). Accurate measurements of the redshift-space

power spectrum will be possible in the linear and mildly nonlinear regime, and a detailed comparison with theoretical predictions will be done in conjunction with the measurement of BAOs. Detailed measurements of redshift space distortions offer an independent test of the growth history of the peculiar velocity field (i.e., Newtonian gravitational potential). This encloses cosmological information on DE (and/or modified gravity), complementary to that in BAO, which measures the background history. A decomposition of the two-point correlation function in the radial and transverse directions also allows for a measurement of bias b and the amplitude of matter clustering σ_8 , which can be used to study the growth history of density fluctuations to $z = 1$. Measurement of the amplitude of the galaxy power spectrum, $P(k)$, as a function of redshift can also be used to determine the growth rate of structure through the cross-correlation of the galaxy data with future CMB lensing data or by using higher-order correlations to determine the bias parameter as a function of scale and redshift. Higher-order correlations, such as the three-point function or bispectrum, can also be used to measure the BAO feature.

5.2.2. Weak Lensing

Weak lensing is sensitive to both the distance and the growth factor as a function of redshift. The lensing effect can be measured using either the shear or the magnification. The PAU camera will not be optimized to measure galaxy ellipticities, so weak lensing shear may not be as good as those from other surveys. However, the accurate photometric redshifts obtained in PAU may be combined with ellipticity measurements obtained in other surveys for the same galaxies. This additional information will help separating shear lensing from intrinsic galaxy alignment.

Gravitational lensing modulates the observed spatial distribution of galaxies. Dim galaxies that otherwise would not have been detected are brought into the sample by the lensing magnification. This increases the observed number density of galaxies. On the other hand, magnification also increases the apparent area, which leads to a drop in the observed number density of

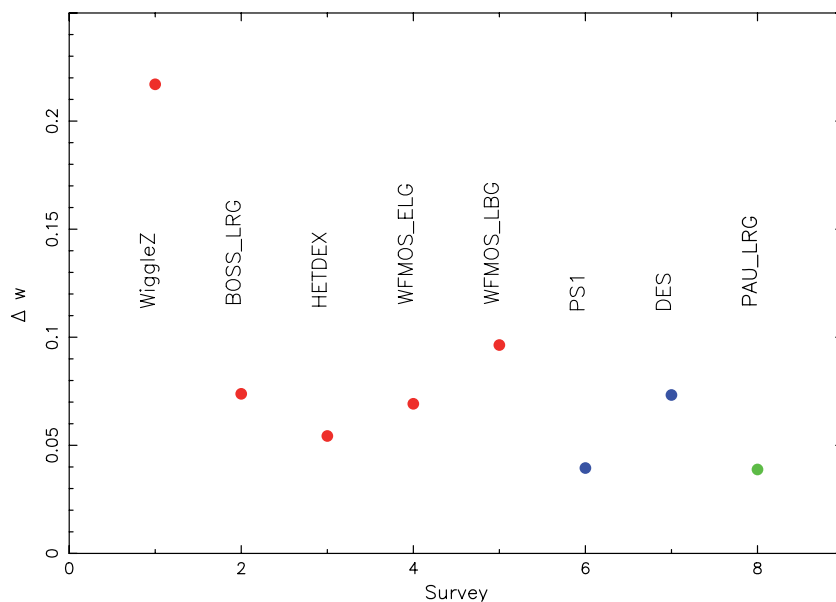


Figure 18. Precision on w (assumed constant) for different proposed ground-based BAO Surveys. All other cosmological parameters are kept fixed, therefore the overall scale is unrealistic, but the relative reach of the different proposals should be realistic. Details about the inputs for the calculations can be found in Table 2. (A color version of this figure is available in the online journal.)

galaxies. The net lensing effect, known as magnification bias, is controlled by the slope of the number counts. The PAU Survey will be able to measure this effect by cross-correlating galaxy samples defined by separated redshift slices.

5.2.3. Galaxy Clusters

Galaxy clusters are the largest collapsed structures in the universe, containing up to hundreds or thousands of individual galaxies. The redshift distribution and the evolution of clustering of massive clusters of galaxies can provide a direct measurement of the cosmic volume as a function of redshift as well as the growth rate of density perturbations. This is complementary to the measurement of the BAO scale, which is purely geometrical in nature. Comparison of theory to observations requires a calibration of the cluster masses (or at least the mass threshold of each cluster sample). Clusters of galaxies can be identified optically by searching for concentrations of galaxies with the same color. The PAU Survey by itself will provide a new window for accurate optical cluster detection and selection, based on the combination of photometric colors and good photo- z precision over all galaxies around each cluster, which will help improving on cluster completeness and contamination. PAU will also provide the opportunity to self-calibrate the mass threshold of a given cluster sample in different ways, such as stacking weak lensing magnification measurements over the cluster positions or using the (biased) amplitude of clustering in the same cluster sample. The photo- z accuracy for clusters will be improved in comparison to the galaxy photo- z by the square root of the number of galaxies in the cluster. This will result in a typical photo- z accuracy which is a few times smaller than that for galaxies. At the same time, one could use the velocity dispersion of the galaxies in each cluster to provide an estimate of the cluster mass. This will not be accurate for individual clusters, but should be accurate enough to have an estimate of the mass threshold of a given cluster sample.

A cluster survey carried out over the PAU area also constrains cosmology through the spatial clustering of the galaxy clusters. As mentioned above, this can be done with even higher

photo- z accuracy than in the PAU galaxy survey. The clustering of galaxy clusters reflect the underlying clustering in the DM; these correlations contain a wealth of cosmological information, much like the information contained in the LRG correlation function, including the BAO position. Even if the number density for clusters is lower than that of LRGs, this is partially compensated by the higher (biased) clustering amplitude. We plan to use the PAU cluster redshift distribution and the cluster power spectrum and clustering as cosmological probes to study the density and nature of the DE.

PAU can also be used in combination with other surveys to provide accurate photo- z in a sample of clusters detected by the Sunyaev–Zel’dovich (SZ) or X-ray signatures of hot gas in clusters, as well as in weak lensing cluster selection.

5.3. Other Science

The large number of narrow filters in the PAU Survey will yield many colors for all the detected galaxies, allowing the measurement of numerous interesting parameters for the study of galaxy evolution: stellar mass, stellar age distribution, metallicity, dust absorption, and interstellar gas emission. This will make possible a detailed study of the rates of star formation, galaxy mergers, and chemical evolution that can account for the evolution of the stellar contents of galaxies of different types, as a function of their environment.

The PAU Survey will substantially increase the sensitivity of astronomical observations to the presence of intergalactic dust, and possibly detect and characterize it for the first time. Intergalactic dust extinction can be searched for by correlating the foreground density of galaxies with the background surface brightness of sources, as well as the extinction measured from our multiple colors. Our accurate photometric redshifts will allow for a good estimate of the mass column density (which should presumably correlate with dust extinction) in the line of sight to every background galaxy. A detailed extinction curve for intergalactic dust may be measurable with our multiple narrow-band colors. The presence of gray dust (causing extinction with no reddening) could also be explored.

The narrow filters of PAU will result in an improved separation of quasars and stars compared to other surveys, and also a more accurate estimate of quasar redshifts from the photometry. Our narrow-band photometry may also be useful to study the mean transmission of the Ly α forest on large scales, its fluctuations, and its evolution with redshift. Quasar lens candidates can be searched for by checking for the presence of multiple images and followed up at another observatory with higher angular resolution. The PAU Survey will also provide a map of galaxies in the vicinity of the lines of sight of all our quasars, with rather accurate photometric redshifts for all the galaxies. One can follow up with spectroscopic observations of a selected sample of quasars at another observatory, and use the PAU galaxies to correlate absorption systems seen in the quasar spectra with the galaxies, to study the distribution of gas around galaxies.

The most luminous star-forming galaxies at redshifts $z \gtrsim 2.5$ will be detectable with the PAU Survey narrow-band photometry by means of their Lyman continuum break, the Ly α forest absorption, and possibly a Ly α emission line. This will allow the study of this galaxy population and its clustering properties over an unprecedentedly large volume.

By selecting the PAU filters appropriately, several parameters of the stars observed in our survey should be measurable, such as effective temperature, surface gravity, iron abundance, and α/Fe . An accurate determination of the density profile and metallicity distribution of halo stars in the Milky Way may follow: the PAU Survey could yield the largest number of metallicity measurements of halo stars, characterizing the stellar populations of the various streams believed to have originated our stellar halo. Giant stars may be also detected by PAU at distances up to ~ 1 Mpc. This could provide our first substantial sample of stars far from any galaxy in the Local Group, and extend the measurements of the halo profile of the Milky Way and its metallicity distributions to much larger radii. For this purpose, it is necessary to have good ways of distinguishing nearby K and M dwarfs from distant K and M giants with the PAU narrow-band photometry.

PAU should also be great for serendipitous discoveries. We will have spectral information for every one of the 10^9 pixels in the survey, which will allow for search of diffuse, low S/N, components, or rare new objects. For example, if there exist any objects in the universe that produce bursts and emit most of their power in an emission line, the PAU Survey will be ideal for discovering them.

6. SUMMARY AND CONCLUSIONS

In 1998, the discovery of the accelerated expansion of the universe changed completely our understanding of the universe and its components. Ten years on, the quest to understand what causes the acceleration continues. Along the way, the BAO technique has been identified as a systematically robust, yet statistically powerful, probe of DE properties. In particular, measuring the BAO feature along the line of sight as a function of redshift provides a direct determination of $H(z)$, which, in turns, depends on the amount and characteristics of DE. However, such a measurement requires a very precise determination of galaxy redshifts.

We have presented here a novel approach to photometric redshift determination which allows the measurement of the BAO feature along the line of sight in an efficient way, by using a set of about 40 narrow-band (FWHM ≈ 100 Å) filters. The approach complements (for BAOs and for other science)

spectroscopic surveys, which typically measure much more precisely the spectra of a much reduced sample of galaxies.

Because of the intrinsic width of the peak in the galaxy–galaxy correlation function of about $15 \text{ Mpc } h^{-1}$, there is a fundamental limitation as to how much one can improve the BAO measurement by reducing the photo- z errors. A redshift precision of order $\sigma(z) \approx 0.003(1+z)$, corresponding to $15 \text{ Mpc } h^{-1}$ along the line of sight at $z = 0.5$, is about optimal for this measurement. Redshift space distortions, biasing, and nonlinear effects produce distortions that can be comparable to the effect of this photo- z precision.

Simulations show that both the target galaxy density ($n \sim 10^{-3} h^3 \text{ Mpc}^{-3}$) and precision in redshift ($\sigma_z/(1+z) \sim 0.003$) can be achieved with the proposed system. These simulations indicate that PAU by itself can determine the equation of state of the DE assumed constant (w) to about 5%, while when the PAU data is combined with expected supernova and CMB data samples, a sizable increase in the DETF figure-of-merit (inverse of the area of the error ellipse in the w_0-w_a plane) by about a factor of 3 is achieved, making the PAU very competitive when compared to other planned ground-based BAO Surveys, photometric or spectroscopic.

The survey will produce a unique data set with low-resolution spectroscopy in the optical wavelengths for all objects in the northern sky up to $m_{AB} = 23-23.5 \text{ arcsec}^{-2}$ (5σ). A survey like PAU, producing such a catalog, will have enormous legacy value and will be extremely useful for many areas of astrophysics, with contributions that are different from, and complementary to, those a spectroscopic survey can deliver.

This work was carried out in the framework of the PAU Consolider Collaboration, supported in part by the Spanish Ministry of Education and Science (MEC) through the Consolider Ingenio-2010 program, under project CSD2007-00060 “Physics of the Accelerating Universe (PAU).” Additional support comes from the Barcelona Supercomputer Center, as well as from the European Commission, the Spanish High Council for Scientific Research (CSIC), and the regional governments of Andalusia, Aragon, Catalonia, Madrid, and Valencia.

REFERENCES

- Adelman-McCarthy, J. K., et al. 2008, *ApJS*, **175**, 297
 ADEPT 2008, http://www7.nationalacademies.org/ssb/BE_Nov_2006_bennett.pdf
 Albrecht, A., et al. 2006, arXiv:astro-ph/0609591
 Angulo, R. E., Baugh, C. M., Frenk, C. S., & Lacey, C. G. 2008, *MNRAS*, **383**, 755
 Astier, P., et al. 2006, *A&A*, **447**, 31
 Basett, B., et al. 2005, arXiv:astro-ph/0510272
 Baum, W. A. 1962, in Proc. IAU Symp. 15, Problems of Extra-Galactic Research, ed. G. C. McVittie (New York: Macmillan), 390
 Benítez, N. 2000, *ApJ*, **536**, 571
 Benítez, N., et al. 2004, *ApJS*, **150**, 1
 Benítez, N., et al. 2008, *ApJL*, in press
 Blake, C., & Bridle, S. 2005, *MNRAS*, **363**, 1329
 Blake, C., Collister, A., Bridle, S., & Lahav, O. 2007, *MNRAS*, **374**, 1527
 Blake, C., & Glazebrook, K. 2003, *ApJ*, **594**, 665
 Blakeslee, J. P., et al. 2003, *ApJ*, **596**, L143
 BOSS 2008, <http://www.sdss.org/news/releases/20080110.sdss3.html>
 Brown, M. J. I., Dey, A., Jannuzi, B. T., Brand, K., Benson, A. J., Brodwin, M., Croton, D. J., & Eisenhardt, P. R. 2007, *ApJ*, **654**, 858
 Budavári, T., Szalay, A. S., Connolly, A. J., Csabai, I., & Dickinson, M. 2000, *AJ*, **120**, 1588
 Cabre, A., & Gaztanaga, E. 2008, *MNRAS*, in press
 Capak, P., et al. 2007, *ApJS*, **172**, 99
 Chevallier, M., & Polarski, D. 2001, *Int. J. Mod. Phys.*, **D10**, 213
 Coe, D., Benítez, N., Sánchez, S. F., Jee, M., Bouwens, R., & Ford, H. 2006, *AJ*, **132**, 926

- Cole, S., et al. 2005, *MNRAS*, **362**, 505
- Cool, R. J., Eisenstein, D. J., Johnston, D., Scranton, R., Brinkmann, J., Schneider, D. P., & Zehavi, I. 2006, *AJ*, **131**, 736
- Crocce, M., & Scoccimarro, R. 2008, *Phys. Rev. D*, **77**, 023533
- D'Abrusco, R., Staiano, A., Longo, G., Brescia, M., Paolillo, M., De Filippis, E., & Tagliaferri, R. 2007, *ApJ*, **663**, 752
- DES 2008, <http://www.darkenergysurvey.org>
- Dickinson, C., et al. 2004, *MNRAS*, **353**, 732
- Eisenstein, D. J., & Hu, W. 1998, *ApJ*, **496**, 605
- Eisenstein, D. J., et al. 2003, *ApJ*, **585**, 694
- Eisenstein, D. J., et al. 2005, *ApJ*, **633**, 560
- Feldman, H. A., Kaiser, N., & Peacock, J. A. 1994, *ApJ*, **426**, 23
- Fosalba, P., Gaztañaga, E., Castander, F., & Manera, M. 2007, arXiv:0711.1540
- Gaztanaga, E., Cabre, A., & Hui, L. 2008, arXiv:0807.3551
- Glazebrook, K., et al. 2007, in ASP Conf. Ser. 379, Proc. Durham "Cosmic Frontiers" Conf., ed. N. Metcalfe & T. Shanks (San Francisco, CA: ASP), 72
- HETDEX 2008, <http://www.as.utexas.edu/hetdex>
- Hickson, P., Gibson, B. K., & Callaghan, K. A. S. 1994, *MNRAS*, **267**, 911
- Hildebrandt, H., Wolf, C., & Benítez, N. 2008, *A&A*, **480**, 703
- Hill, G. J., Gebhardt, K., Komatsu, E., & MacQueen, P. J. 2004, in AIP Conf. Proc., 743, The New Cosmology Conference on Strings and Cosmology (New York: AIP), 224
- Hinshaw, G. 2008, arXiv:0803.0732v1
- Holland, S. E., Groom, D. E., Palaio, N. P., & Wei, M. 2003, *IEEE Trans. Electron. Dev.*, **ED-50**, 225
- Homeier, N. L., et al. 2006, *ApJ*, **647**, 256
- Hütsi, G. 2006a, *A&A*, **449**, 891
- Hütsi, G. 2006b, *A&A*, **459**, 375
- Jones, W. C., et al. 2006, *ApJ*, **647**, 823
- Kaiser, N. 1987, *MNRAS*, **227**, 1
- Komatsu, E., et al. 2008, arXiv:0803.0547
- Leach, B., & Low, F. J. 2000, in Proc. SPIE 4008, CCD and IR Array Controllers, ed. M. Iye & A. F. Moorwood (Bellingham, WA: SPIE), 337
- Linder, E. V. 2003, *Phys. Rev. Lett.*, **90**, 091301
- Martínez, V. J., & Saar, E. 2002, *Statistics of the Galaxy Distribution* (Boca Raton, FL: Chapman and Hall)
- Moles, M., et al. 2005, arXiv:astro-ph/0504545
- Moles, M., et al. 2008, *AJ*, **136**, 1325
- Okumura, T., Matsubara, T., Eisenstein, D. J., Kayo, I., Hikage, C., Szalay, A. S., & Schneider, D. P. 2008, *ApJ*, **676**, 889
- Oyaizu, H., Lima, M., Cunha, C. E., Lin, H., Frieman, J., & Sheldon, E. S. 2008, *ApJ*, **674**, 768
- Padmanabhan, N., & White, M. 2008, *Phys. Rev. D*, **77**, 123540
- Padmanabhan, N., et al. 2007, *MNRAS*, **378**, 852
- Pan-STARRS 2008, <http://pan-starrs.ifa.hawaii.edu/public/>
- Patat, F. 2004, *The Messenger*, **115**, 1
- Peacock, J. A., et al. 2006, arXiv:astro-ph/0610906
- Percival, W. J., Cole, S., Eisenstein, D. J., Nichol, R. C., Peacock, J. A., Pope, A. C., & Szalay, A. S. 2007, *MNRAS*, **381**, 1053
- Percival, W., et al. 2007, *ApJ*, **657**, 645
- Puxley 2008, <http://www.gemini.edu/sciops/ObsProcess/obsConstraints/ocSkyBackground.html>
- Readhead, A. C. S., et al. 2004, *ApJ*, **609**, 498
- Reichardt, C. L., et al. 2008, arXiv:0801.1491
- Riess, A., et al. 2007, *ApJ*, **659**, 98
- Ross, N. P., et al. 2007, *MNRAS*, **381**, 573
- Sánchez, S. F., Thiele, V., Aceituno, J., Cristobal, D., Perea, J., & Alves, J. 2008, *PASP*, **120**, 1244
- Seo, J. J., & Eisenstein, D. J. 2003, *ApJ*, **598**, 720
- Silk, J. 1968, *ApJ*, **151**, 459
- SPACE 2008, <http://sci.esa.int/science-e/www/object/index.cfm?fobjectid=42266>
- Spergel, D., et al. 2007, *ApJS*, **170**, 377
- Springel, V. 2005, *MNRAS*, **364**, 1105
- Starr, B. M., et al. 2004, in *Scientific Detectors for Astronomy, Astrophysics and Space Science Library 300, Monsoon Image Acquisition System* ed. P. Amico, J. N. Beletic, & J. E. Beletic (Netherlands: Springer), 269
- Sterken, C. (ed.) 2007, in ASP Conf. Ser. 364, *The Future of Photometric, Spectrophotometric and Polarimetric Standardization* (San Francisco, CA: ASP)
- Tegmark, M., et al. 2004, *ApJ*, **606**, 702
- Tegmark, M., et al. 2006, *Phys. Rev. D*, **74**, 123507
- Walker, A. 1987, *NOAO Newslett.*, **10**, 16
- WiggleZ 2008, <http://astronomy.swin.edu.au/karl/Karl-Home/Home.html>
- Wolf, C., Meisenheimer, K., Rix, H.-W., Borch, A., Dye, S., & Kleinheinrich, M. 2003, *A&A*, **401**, 73
- Wolf, C., et al. 2001, *A&A*, **365**, 681
- Wood-Vasey, W. M., et al. 2007, *ApJ*, **666**, 694